REPORT DOCUMENTATION PAGE

Form Approved OMB NO. 0704-0188

1. REPORT DATE (DD-MM-YYYY)	2. REPORT TYPE	3. DATES COVERED (From - To)
08-07-2015	Final Report	10-May-2009 - 9-Nov-2013

4. TITLE AND SUBTITLE
Final Report: Molecular Level Understanding of Electrocatalysis in High pH Environment

5a. CONTRACT NUMBER
W911NF-09-1-0227

5b. GRANT NUMBER

5c. PROGRAM ELEMENT NUMBER
611102

6. AUTHORS
Sanjeev Mukerjee, Nagappan Ramaswamy, Qinggang He, Daniel Abbott

5d. PROJECT NUMBER

5e. TASK NUMBER

5f. WORK UNIT NUMBER

7. PERFORMING ORGANIZATION NAMES AND ADDRESSES
Northeastern University
360 Huntington Ave
490 RP
Boston, MA 02115 -5005

8. PERFORMING ORGANIZATION REPORT NUMBER

9. SPONSORING/MONITORING AGENCY NAME(S) AND ADDRESS (ES)
U.S. Army Research Office
P.O. Box 12211
Research Triangle Park, NC 27709-2211

10. SPONSOR/MONITOR'S ACRONYM(S)
ARO

11. SPONSOR/MONITOR'S REPORT NUMBER(S)
55036-CH.9

12. DISTRIBUTION AVAILIBILITY STATEMENT
Approved for Public Release; Distribution Unlimited

13. SUPPLEMENTARY NOTES
The views, opinions and/or findings contained in this report are those of the author(s) and should not contrued as an official Department of the Army position, policy or decision, unless so designated by other documentation.

14. ABSTRACT
This effort involved the synthesis of novel electrocatalysts for both anodic oxidation of complex fuels (especially directed towards facile breakage of C-C bond) and cathodic oxygen reduction reaction in alkaline environment for intended application in alkaline anion exchange membrane fuel cell. This was facilitated by an array of electrochemical and spectroscopic investigations. This project provides a holistic understanding of the anion exchange ionomer interaction with the electrocatalyst of choice from the point of view of double layer and the operating potential. Among the principle contributions made in this project are: (1) Unified mechanism of

15. SUBJECT TERMS
Alkaline Fuel Cells, Electrocatalysts, In situ Spectroscopy

16. SECURITY CLASSIFICATION OF:			17. LIMITATION OF ABSTRACT	15. NUMBER OF PAGES	19a. NAME OF RESPONSIBLE PERSON
a. REPORT	b. ABSTRACT	c. THIS PAGE			Sanjeev Mukerjee
UU	UU	UU	UU		19b. TELEPHONE NUMBER 617-373-2382

Report Title

Final Report: Molecular Level Understanding of Electrocatalysis in High pH Environment

ABSTRACT

This effort involved the synthesis of novel electrocatalysts for both anodic oxidation of complex fuels (especially directed towards facile breakage of C-C bond) and cathodic oxygen reduction reaction in alkaline environment for intended application in alkaline anion exchange membrane fuel cell. This was facilitated by an array of electrochemical and spectroscopic investigations. This project provides a holistic understanding of the anion exchange ionomer interaction with the electrocatalyst of choice from the point of view of double layer and the operating potential. Among the principle contributions made in this project are: (1) Unified mechanism of electrocatalysis at an alkaline electrolyte interface, with detailed activity descriptors defining the structure of active site required for concerted inner sphere four electron reduction of oxygen. (2) Provided details on interfacial interactions of anion exchange membrane ionic exchange site and choice of electrocatalysts. (3) Initiation of a new initiative for advancing fundamental understanding of plasmonic enhancement of charge transfer at an electrochemical interface. Initial preliminary data proves this concept to be true and highly sensitive to the generation of surface plasmons and quantum confinement in nano-particles such as Au.

Enter List of papers submitted or published that acknowledge ARO support from the start of the project to the date of this printing. List the papers, including journal references, in the following categories:

(a) Papers published in peer-reviewed journals (N/A for none)

Received	Paper

TOTAL:

Number of Papers published in peer-reviewed journals:

(b) Papers published in non-peer-reviewed journals (N/A for none)

Received	Paper
07/08/2013 5.00	Iromie Gunasekara, Myoungseok Lee, Daniel Abbott, Sanjeev Mukerjeez. Mass Transport and Oxygen Reduction Kinetics at an Anion Exchange Membrane Interface: Microelectrode Studies on Effect of Carbonate Exchange, ECS Electrochemistry Letters, (03 2012): 0. doi:
07/08/2013 7.00	Murat Ünlü, Daniel Abbott, Nagappan Ramaswamy, Xiaoming Ren, Sanjeev Mukerjee, Paul A. Kohl. Analysis of Double Layer and Adsorption Effects at the Alkaline Polymer Electrolyte-Electrode Interface, Journal of the Electrochemical Society, (06 2011): 0. doi:
07/12/2013 8.00	Qinggang He, Badri Shyam, Katerina Macounova, Petr Krtil, David Ramaker, Sanjeev Mukerjee. Dramatically Enhanced Cleavage of the C-C Bond Using an Electrocatalytically Coupled Reaction, Journal of the American Chemical Society, (04 2012): 0. doi:

TOTAL: **3**

Number of Papers published in non peer-reviewed journals:

(c) Presentations

Number of Presentations: 0.00

Non Peer-Reviewed Conference Proceeding publications (other than abstracts):

Received Paper

TOTAL:

Number of Non Peer-Reviewed Conference Proceeding publications (other than abstracts):

Peer-Reviewed Conference Proceeding publications (other than abstracts):

Received Paper

TOTAL:

Number of Peer-Reviewed Conference Proceeding publications (other than abstracts):

(d) Manuscripts

Received		Paper
07/08/2013	6.00	Nagappan Ramaswamy, Urszula Tylus, Qingying Jia, Sanjeev Mukerjee. Activity Descriptor Identification for Oxygen Reduction on Non-Precious Electrocatalysts: Linking Surface Science to Coordination Chemistry, SUBMITTED (06 2013)
09/20/2011	2.00	Nagappan Ramaswamy, and Sanjeev Mukerjee. Influence of Inner and Outer-Sphere Electron Transfer Mechanisms during Electrocatalysis of Oxygen Reduction in Alkaline Media, Journal of Physical Chemistry C (01 2011)
09/20/2011	3.00	Nagappan Ramaswamy, Robert J. Allen and Sanjeev Mukerjee. Electrochemical Kinetics and X-ray Absorption Spectroscopic Investigations of Oxygen Reduction on Chalcogen Modified Ruthenium Catalysts in Alkaline Medium, Journal of Physical Chemistry C (09 2011)
TOTAL:		**3**

Number of Manuscripts:

Books

Received		Book
07/08/2013	4.00	Sanjeev Mukerjee, Nagappan Ramaswamy. Fundamental Mechanistic Understanding of Electrocatalysts of Oxygen Reduction on Pt and Non-Pt Surfaces: Acid versus Alkaline Media, New York: Hindawi Publishing Corporation, (12 2012)
TOTAL:		**1**

Received	Book Chapter

TOTAL:

Patents Submitted

Non Noble Metal Electrocatalysts and Their Uses', US Patent Office Application, S. Mukerjee and U. Tylus, PCT/US14/10502, filed 1/7/2014

- 'Non Noble Metal Based ODC Cathodes for Chlorine Evolution Process', S. Mukerjee and U. Tylus, App # 61/749,650 (2014)

Patents Awarded

Awards

- Elected Fellow of the Electrochemical Society (Fall 2013).
- Research and Creativity award at Northeastern University (2013).
- Ford Motor Co., University Professor Award (2013)

Graduate Students

NAME	PERCENT_SUPPORTED	Discipline
Nagappan Ramaswamy	1.00	
Qinggang He	1.00	
Daniell Abbott	0.25	
Urszula Tylus	0.25	
FTE Equivalent:	**2.50**	
Total Number:	**4**	

Names of Post Doctorates

NAME	PERCENT_SUPPORTED
FTE Equivalent:	
Total Number:	

Names of Faculty Supported

NAME	PERCENT_SUPPORTED	National Academy Member
Sanjeev Mukerjee	0.28	
FTE Equivalent:	**0.28**	
Total Number:	**1**	

Names of Under Graduate students supported

NAME	PERCENT_SUPPORTED
FTE Equivalent:	
Total Number:	

Student Metrics

This section only applies to graduating undergraduates supported by this agreement in this reporting period

The number of undergraduates funded by this agreement who graduated during this period:	0.00
The number of undergraduates funded by this agreement who graduated during this period with a degree in science, mathematics, engineering, or technology fields:.....	0.00
The number of undergraduates funded by your agreement who graduated during this period and will continue to pursue a graduate or Ph.D. degree in science, mathematics, engineering, or technology fields:.....	0.00
Number of graduating undergraduates who achieved a 3.5 GPA to 4.0 (4.0 max scale):.....	0.00
Number of graduating undergraduates funded by a DoD funded Center of Excellence grant for Education, Research and Engineering:.....	0.00
The number of undergraduates funded by your agreement who graduated during this period and intend to work for the Department of Defense	0.00
The number of undergraduates funded by your agreement who graduated during this period and will receive scholarships or fellowships for further studies in science, mathematics, engineering or technology fields:	0.00

Names of Personnel receiving masters degrees

NAME
Total Number:

Names of personnel receiving PHDs

NAME	
Nagappan Ramaswamy	
Qinggang He	
Daniel Abbott	
Urszula Tylus	
Total Number:	**4**

Names of other research staff

NAME	PERCENT_SUPPORTED
FTE Equivalent:	
Total Number:	

Sub Contractors (DD882)

Inventions (DD882)

Scientific Progress

Technology Transfer

Non PGM catalyst technology tranferred to Pajarito powders for scale up.
Process of transferring the ODC catalyst patents to Denora North Americal

Final Project Report- Grant # 55036-CH
(Reporting Period: September 2009-14)

Effort Title: Molecular Level Understanding of Electrocatalysis in High pH Environment

PI Name: Sanjeev Mukerjee
Department: Chemistry and Chemical Biology
Institution, City, State, Zip: Northeastern University, Boston, MA, 02115

Objective

Synthesize novel electrocatalysts for both anodic oxidation of complex fuels (especially directed towards facile breakage of C-C bond) and cathodic oxygen reduction reaction in alkaline environment for intended application in alkaline anion exchange membrane fuel cell. Further, perform an array of electrochemical and spectroscopic investigations on the catalysts developed for a thorough structure property relationship. Provide a holistic understanding of the anion exchange ionomer interaction with the electrocatalyst of choice from the point of view of double layer and the operating potential. At the end of the program a further objective was to investigate the potential of plasmonic enhancement of charge transfer at an electrochemical interface.

Approach

The overall approach is constitutes

(a) Synthesis of electrocatalysts, both supported and unsupported on various carbon blacks using a variety of novel synthetic approaches.
(b) Screening of activity using a specially designed RRDE set up to investigate the kinetic parameters and parallel electron transfer step (at the ring electrode) while avoiding the interference from factors such as carbonate formation (in the case of anodic oxidation of alcohols) using specially designed protocols. These include ability to make extremely thin and uniform film deposits on glassy carbon substrates as well as efficient removal of CO_2 from the interface via improved diffusion flux to the electrode tip in the RRDE.
(c) Conducting *in situ* synchrotron X-ray absorption spectroscopy (XAS) spectroscopy on select electrocatalysts, especially those found promising for oxidation of complex alcohols, such as ethanol. *The progression of conventional XAS spectroscopy from being a bulk averaging technique to a more surface specific probe using the near edge part of the spectra (X-ray absorption near edge structure, XANES), referred to as the 'Delta μ Technique' forms the corner stone to the successful elucidation of structure property relationships.*
(d) Conducting strategic single cell studies for measuring steady state polarization and determination of Tafel kinetics.
(e) Conducting in situ plasmonic experiments in aqueous and non-aqueous medium to evaluate the potential of engendering plasmonic enhancement of charge transfer, especially those involving and outer sphere mechanism.

Relevance to Army

The combination of characteristics of alkaline fuel cells such as low temperature, silent operation and absence of poisonous exhausts make them apt for defense applications since such features make them difficult to detect by common acoustic and infrared detection techniques[1]. Areas of defense applications for alkaline membrane fuel cell can be broadly envisaged as light weight, solid state, portable soldier & sensor power, high power electric combat vehicles, stationary

power for base camps etc., Silent operation (compared to combustion engine-generator sets) and longer running time (compared to batteries) are examples of unique combination of alkaline fuel cell features. Also these fuel cells can be used to recharge batteries where no grid is available and combustion engine generators could be harmful

Accomplishments for Reporting Period

Detailed, bulleted accomplishments for the period should be traceable back to approach and objectives please be specific and quantitative where possible.

- Unified mechanism of electrocatalysis at an alkaline electrolyte interface, with detailed activity descriptors defining the structure of active site required for concerted inner sphere four electron reduction of oxygen.
- Provided details on interfacial interactions of anion exchange membrane ionic exchange site and choice of electrocatalysts.
- Initiation of a new initiative for advancing fundamental understanding of plasmonic enhancement of charge transfer at an electrochemical interface. Initial preliminary data proves this concept to be true and highly sensitive to the generation of surface plasmons and quantum confinement in nano-particles such as Au.

Collaborations and Technology Transfer

- 'Non Noble Metal Electrocatalysts and Their Uses', US Patent Office Application, S. Mukerjee and U. Tylus, PCT/US14/10502, filed 1/7/2014
- 'Non Noble Metal Based ODC Cathodes for Chlorine Evolution Process', S. Mukerjee and U. Tylus, App # 61/749,650 (2014)

Resulting Journal Publications During Reporting Period.

1. 'Analysis of Double Layer and Adsorption Effects at the Alkaline Polymer Electrolyte Interface', M. Unlu, D. Abbott, N. Ramaswamy, X. Ren, S. Mukerjee and P. A. Kohl, *J. Electrochem. Soc.,* **158**, B1423 (2011).
2. 'Electrochemical Kinetics and X-ray Absorption Spectroscopic Investigation of Oxygen Reduction on Chalcogen-Modified Ru Catalysts in Alkaline Medium', N. Ramaswamy, R. J. Allen and S. Mukerjee, *J. Phys. Chem. C.,* **115**, 12650 (2011).
3. 'A Novel Non Noble CuFe/C Catalyst for Electroreduction of Oxygen in Alkaline Media', Q. He, X. Yang, X. Ren, B. E. Koel, N. Ramaswamy, S. Mukerjee and R. Kostecki, *J. Power Sources* **196**, 7404 (2011).
4. 'A Novel Non Noble CuFe/C Catalyst for Electroreduction of Oxygen in Alkaline Media', Q. He, X. Yang, X. Ren, B. E. Koel, N. Ramaswamy, S. Mukerjee and R. Kostecki, *J. Power Sources* **196**, 7404 (2011).
5. 'Influence of Inner and Outer Sphere Electron Transfer Mechanisms during Electrocatalysis of Oxygen in Alkaline Medium', N. Ramaswamy and S. Mukerjee, *J. Phys. Chem. C.,* **115**, 18015 (2011).
6. 'The Beneficial Role of Co-Metals Pd and Au in Carbon Supported PtPdAu Catalyst Towards Promoting Ethanol Oxidation Kinetics in Alkaline Fuel Cells: Temperature Effect and Mechanism' J. Datta, A. Dutta and S. Mukerjee, *J. Phys. Chem. C.,* **115**, 15324 (2011).

7. 'Fundamental Mechanistic Understanding of Electrocatalysis of Oxygen Reduction on Pt and Non Pt Surfaces: Acid vs. Alkaline Medium', N. Ramaswamy and S. Mukerjee, *Advances in Physical Chemistry*, **Vol. 2012**, Article ID 491604, (2012).
8. Dramatically Enhanced Cleavage of the C-C Bond Using an Electrocatalytically Coupled Reaction' Q. He, B. Shyam, K. Macounova, P. Krtil, D. Ramaker, S. Mukerjee,**JACS*, **134**, (20) pp 8655-8661 (2012).
9. 'Mass Transport and Oxygen Reduction Kinetics at an Anion Exchange Membrane Interface: Microelectrode Studies on Effect of Carbonate Exchange', I. Gunasekara, M. Lee, D. Abbott and S. Mukerjee, *ECS Electrochemistry Lett.,* **1(2)**, F16-19, (2012).
10. 'Activity Descriptor Identification for Oxygen Reduction on Non-Precious Electrocatalysts: Linking Surface Science to Coordination Chemistry' Nagappan Ramaswamy, Urszula Tylus, Qingying Jia and Sanjeev Mukerjee, *JACS* **135 (41)**, 15443 (2013).

Graduate Students Involved During Reporting Period

- Dr. Nagappan Ramaswamy, graduated 2013, currently employed by General Motors, Pontiac Division.
- Dr. Qinggang He, graduated 2014, currently faculty member at Zhejiang University, PRC.
- Urszula Tylus, (partially supported on this grant), graduated 2014, currently postdoc at Los Alamos National Laboratory.

Awards, Honors and Appointments

- Elected Fellow of the Electrochemical Society (Fall 2013).
- Research and Creativity award at Northeastern University (2013).
- Ford Motor Co., University Professor Award (2013)

Understanding Fundamentals of Solute Transport in Anion Exchange Membranes: Effect of Carbonate ions

Published Article: 'Mass Transport and Oxygen Reduction Kinetics at an Anion Exchange Membrane Interface: Microelectrode Studies on Effect of Carbonate Exchange', I. Gunasekara, M. Lee, D. Abbott and S. Mukerjee, ECS Electrochemistry Lett., 1(2), F16-19, (2012).

A solid state electrochemical cell (with a 100 μm Pt micro-disk as the working electrode, 1.6 mm Pt disc counter electrode and a Dynamic hydrogen reference electrode) was used to study mass transport and kinetics of oxygen reduction reaction (ORR) and hydrogen / methanol oxidation reactions. Experiments for the membrane in the hydroxide form were conducted in a carbon dioxide free environment. Results obtained showed that the carbonate ion exchange in the alkaline membrane greatly affects the kinetics as well as the transport of electro-active species through the membrane. Experimental observations are discussed below.

Results and discussion

Oxygen reduction reaction

Linear sweep voltammetric measurements were carried out for an oxygen saturated membrane at 293 K. Figure 01 A shows the activity comparison of Anion Exchange Membrane (AEM) in carbonate and hydroxide forms, and Nafion-112 membrane at 293 K. Comparison of kinetic currents in Table 01 shows that the ORR currents are not significantly affected by the exchange of the hydroxide ions by carbonate ion.

Potential jump chronoamperometric measurements were recorded and mass transport parameters were calculated using the corresponding Cottrell plots (Figure 1B). Table 02 shows a significant decrease in the mass transport parameters as a result of exchange with carbonate ions. Larger diffusion coefficients are expected for membranes with high ion exchange capacity (Table 02). However low mobility of the carbonate ions inside the membrane pores can interfere with oxygen transport.

Hydrogen oxidation reaction

Activity comparison for the hydrogen oxidation reaction (HOR) at the membrane electrode interface is shown in Figure 02 A. Unlike that for the oxygen reduction reaction, HOR kinetics at the interface are significantly affected when mobile anion in the membrane is changed to carbonate (Table 03). Interference of the carbonate ions to the adsorption of hydroxide ions as well the decrease in OHad concentration on the electrode are the main reasons for the observed low rate of hydrogen oxidation. Hydrogen oxidation reaction was also recorded on membranes coated with 0.4 mg cm-2 of AS4 ionomer (Figure 02 B). Kinetic currents at the membrane – electrode interface are suppressed as a result of ionomer coating. It is interesting that the poisoning effect from the membrane quaternary ammonium species is negligible whereas those from the ionomer quaternary ammonium sites are significant.

Transport of hydrogen molecules also exhibits some interesting insights. Hydrogen permeability in both AEM(OH) and Proton Exchange Membrane(PEM) are similar (Table 04). As expected, carbonate ion exchange has no effect on the diffusion of small hydrogen molecules through the AEM.

Methanol oxidation at the AEM-Pt interface

Methanol oxidation reaction at the membrane electrode interface has been studied using a liquid feed enabled cell. Membrane was equilibrated with 1M MeOH solution in water before electrochemical analysis. Figure 03 A,B compares the activity in hydroxide and carbonate forms

for Tokuyama membranes A-201, A-90 with that of Nafion 112 and aqueous KOH solution (0.1M). According to Table 05, methanol oxidation current at 0.65 V for the Pt / AEM interface drastically decreases as the hydroxide ions are completely replaced by carbonate ions. Tafel plots obtained by steady state voltammetric measurements show a slope of 142 mV dec-1 which increases when the membrane is exchanged to carbonate ions. The decrease in the rate of MOR in carbonate solutions can be attributed to the decreases OHad concentration. Adsorbed carbonate ions on the platinum surface at these potentials clearly imposes some interference on adsorption of methanol molecules. The change in MOR Tafel slopes can be further attributed to mass transfer complications observed in solid polymer electrolytes.

Diffusion and solubility parameters of methanol in membranes obtained by potential jump chronoamperometric measurements are shown in Table 06. Water sorption in the membrane is proportional to the number of charged sites (ion exchange capacity). High water sorption in the AEMs swells the membrane more and the wide water channels facilitate methanol transport. However the reason behind the decrease in transport properties in the carbonated form of the membranes is not clear. Variation in membrane swelling with the radius of the cation/anion has been reported for PEMs. Change in the swelling of the AEM with the change of the ionic species could be the reason for the hindered methanol transport in the carbonate form of the membrane.

Figures and Tables

Table 01: Kinetic parameters for Hxygen reduction reaction

Electrolyte (293K , 1 atm)	jo 109 / A cm-2 (hcd)	αhcd	jo 1010 / A cm-2 (lcd)	αlcd	j 104 at 0.9 V / A cm-2geo
AAEM (Carbonate-Free)	8.28	0.79	2.53	1.02	1.0
AAEM (complete exchange with K2CO3)	1.03	0.72	0.31	1.09	0.3
1.0 M NaOH	--	0.73	0.6	1.32	7.2
Nafion 112	231	0.50	67.7	0.81	2.3
0.1 HClO4	--	0.57	47	0.83	23

Table 02: Comparison of Mass transport characteristics of Oxygen

Electrolyte (293K, 1 atm)	D 10-6 / cm2 s-1	C 10-6 / mol cm-3	DC 10-6 / mol cm-1 s-1	IEC (meq g-1)	Water uptake (w %)	λ
AAEM (Carbonate-Free)	4.29	0.93	3.99	1.8	63	18.5
AEM (complete exchange with K2CO3)	0.23	0.90	0.22	1.8	59	18.2
Nafion 112	0.73	6.5	4.8	0.91	32	19.8

Table 03: Kinetic parameters for Hydrogen oxidation reaction

Electrolyte	jo (mA/cm-2)	Tafel slope (mV dec-1)
0.1 M KOH	0.69	116
AAEM (OH-)	0.67	105
AAEM (CO32-)	0.02	39

Table 04: Comparison of Mass transport characteristics of Hydrogen

Electrolyte	Diffusion coefficient D 106 (cm2 s-1)	Solubility C106 (mol cm-3)	Permeability DC1012 (mol cm-1 s-1)
AAEM-(OH-)	1.34	2.98	4.00
AAEM-(CO32-)	1.30	0.52	0.68
Nafion 117	7.6	0.51	3.9

Table 05: Kinetic parameters for Methanol oxidation reaction

Electrolyte	Tafel Slope mV dec-1	j at 0.65 V 10-5 A cm-2
A201(OH)	142	4.32
A201(CO32-)	314	1.00
A901(OH)	122	15.06
A901(CO32-)	249	1.00
0.1M KOH solution	113	294.4
Nafion 112	138	4.12

Table 06: Comparison of Mass transport characteristics of Methanol in the membranes

Electrolyte	Diffusion coefficient D106 (cm2 s-1)	Solubility C106 (mol cm-3)	Permeability DC1012 (mol cm-1 s-1)
A201-(OH-)	22.4	1.19	26.7
A201- (CO32-)	0.61	1.22	0.74
A901- (OH-)	10.0	2.73	27.35
A901- (CO32-)	8.5	1.68	14.3
Nafion 112	8.0	1.92	15.4

Figure 01: A) Mass transport corrected Tafel plots for the Oxygen reduction reaction at the Pt/ AEM interface, 293K

B) Cottrell plots for ORR calculated from current-time transients at 0.4V (potential jump from 1V to 0.4 V)

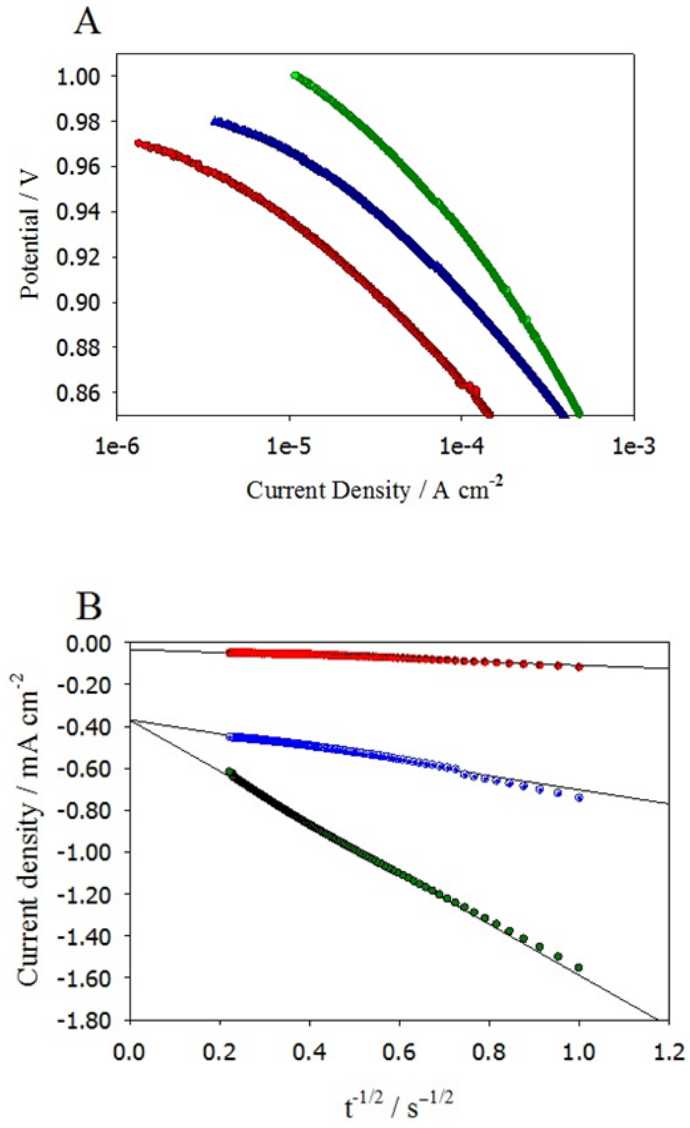

Figure 02: A) Mass transport corrected Tafel plots for the Hydrogen oxidation reaction at the Pt/ AEM interface, 293K
B) Comparison of kinetics in the presence of AS4 ionomer
C) Cottrell plots for the oxygen reduction reaction at 0.4V (potential jump from 1V to 0.4V)

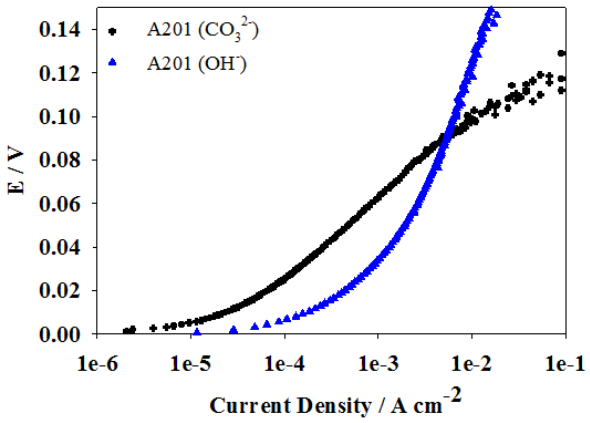

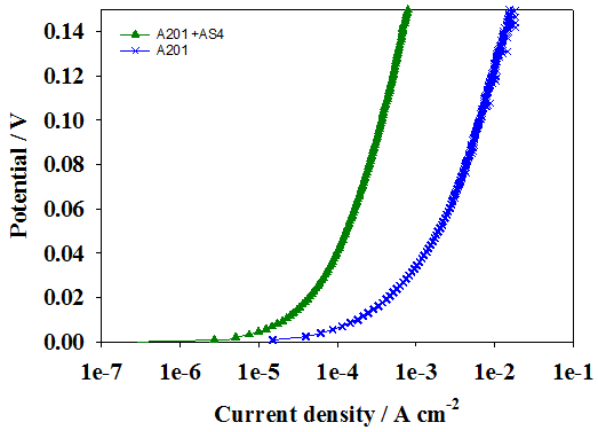

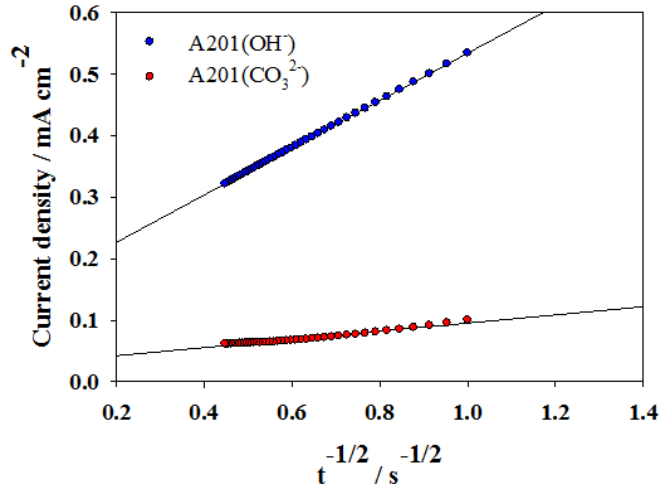

Figure 03: A,B) Mass transport corrected Tafel plots for the Methanol oxidation reaction at the Pt/ AEM interface, 293K

C) Cottrell plots for MOR calculated from current-time transients at 0.8V (potential jump from 0.4V to 0.8 V)

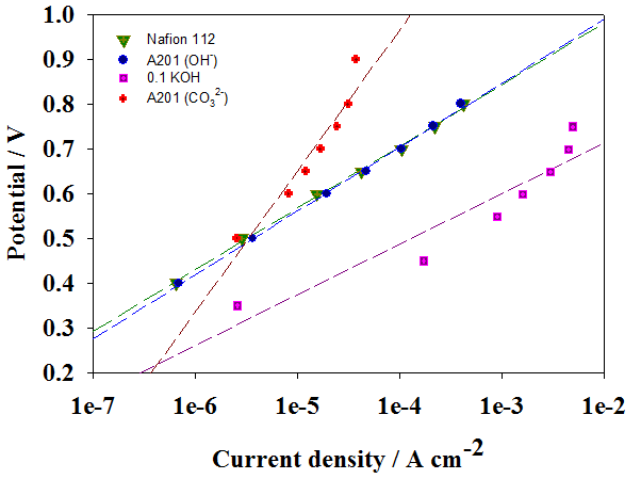

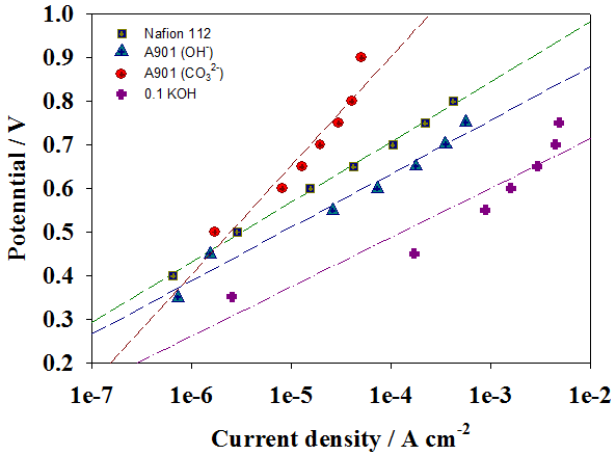

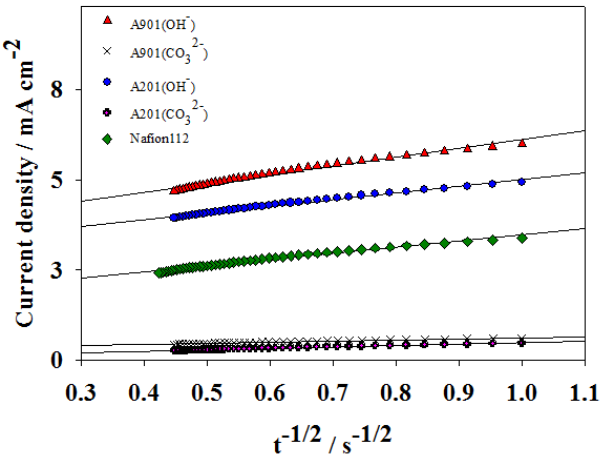

Fundamental Understanding of the Interfacial Double Layer during Direct Alcohol Oxidation

Published Article: 'Analysis of Double Layer and Adsorption Effects at the Alkaline Polymer Electrolyte Interface', M. Unlu, D. Abbott, N. Ramaswamy, X. Ren, S. Mukerjee and P. A. Kohl, *J. Electrochem. Soc.,* **158**, B1423 (2011).

In general, it is well recognized that the addition of alkali metal ions to the electrolyte improves the rate of alcohol oxidation due to the higher pH, indicating that the pH in AEM matrix without the added alkali electrolyte may not be high enough. In addition, it has been proposed that there is an optimum ratio of OH^- to MeOH, which balances the removal of reaction intermediates and surface coverage of methanol and hydroxide. However, a more fundamental understanding of the origin of the limited cell performances in AEM fuel cells remains elusive. Therefore, the primary objective of this research was to unravel the various aspects that influence the charge transfer processes at the anode-alkaline membrane interface.

Experimental Aspects:

Membrane electrode assemblies (MEAs) were prepared using commercial PtRu (Alfa Aesar, 4.0mgPtRu/cm2) or Pt (Alfa Aesar, 2.0 mgPt/cm2) anodes on Toray paper, Pt/C cathode on Gas Diffusion Layer (GDL), Tokuyama AS4 ionomer solution, and Tokuyama A201 ionomer membrane. Commercial PtRu anodes were spray coated with an interfacial layer of 1.0 mgAS4/cm2 of alkaline ionomer on the top surface prior to hot pressing. To prepare the cathode, a catalyst ink composed of BASF 30% Pt/C dispersed in a water-alcohol mixture along with the requisite amount of ionomer (Tokuyama AS4) was sprayed on gas diffusion layer (GDL, ETEK-BASF). Typical cathode loading consisted of 1.0 mgPt/cm2 with an ionomer content of 28.5% by weight of the catalyst. After drying the cathodes, a layer of interfacial ionomer was sprayed to achieve a loading of 1.0 mgAS4/cm2. Hot pressing of the electrodes together with a Tokuyama A-201 membrane was carried out at 60°C and 100 psig pressure for duration of four minutes. MEAs were then assembled in a fuel cell consisting of 5 cm2 serpentine flow fields. Humidification of the MEA was performed for 2 hours by flowing N2 (100% RH) at a cell temperature of 50°C. Higher duration of humidification was not preferred to avoid thermal degradation of the membrane and the ionomer layer. The operating temperature of the cell was typically set at 50°C and the cell was activated with H2/O2 (inlet temperatures of 55°C, 100% RH, 28 psig back pressure).

The hydrogen adsorption/desorption and methanol oxidation experiments on planar Pt disk electrodes were conducted using a traditional three-electrode cell at ambient temperature. The Pt disk electrode had a geometric surface area of 0.385 cm2. The Pt electrode surface was polished with a 0.05 μm alumina slurry and sonicated in distilled water for 10 minutes. The electrode was then soaked in concentrated nitric acid and rinsed thoroughly. Ag/AgCl was the reference electrode and carbon cloth was used as the counter electrode. Tetramethylammonium hydroxide (TMAOH), sodium hydroxide (NaOH), and poly(diallyldimethylammonium hydroxide) (PTMAOH) were used as electrolytes. PTMAOH was prepared from

poly(diallyldimethylammonium chloride) using an ion exchange column. The electrolyte solutions were stored under nitrogen to prevent contamination from atmospheric carbon dioxide. The flow of nitrogen over the solution was maintained throughout the experiments. The solutions were purged with nitrogen for 30 minutes before the electrode was immersed into solution. The electrode surface was equilibrated by sweeping the potential at a scan rate of 100 mV/s until steady-state behavior was obtained, ca. 25 cycles. Electrochemical measurements were made using a PAR Potentiostat/Galvonostat Model 2273.

Ammonium contamination studies were conducted on Pt/C modified glassy carbon electrodes. A catalyst ink was prepared from 25 mg of 30% Pt/C (BASF) in 10 mL Millipore H2O and 10 mL isopropyl alcohol. Exactly 5 μL of ink was deposited on a glassy carbon rotating disk electrode (Ageo = 0.247 cm2) to yield a total catalyst loading of 7.5 μgPt/cm2. Prior to ink deposition, the electrode was polished with 0.05 μm alumina slurry and sonicated twice in a sonic bath for 30 seconds each in a 50:50 solution of Millipore H2O and isopropyl alcohol. The reference electrode used was a reversible hydrogen electrode (RHE) prepared from a solution of 0.1 M KOH. At the beginning of each experiment, the electrode was cycled 20 times from 0.05 V to 1.2 V at 50 mV/s in 0.1 M KOH followed by five cycles at 20 mV/s. Absolute methanol was then added to the KOH solution to obtain a total MeOH concentration of 0.5 M. Methanol oxidation was then performed by holding the potential at 0.6 V vs. RHE for 900 seconds. Subsequently, an aliquot of a given contaminant was added to bring the total contaminant concentration to 1 mM and the potential was again held at 0.6 V for 900 seconds. This procedure was repeated for the remaining contaminant concentrations of 5, 10, 20, 40, 60, and 120 mM. A new ink coating was used in the study of each contaminant. Contaminants investigated included tetramethylammonium hydroxide (TMAOH, 25% w/w aq) , tetraethylammonium hydroxide (TEAOH, 35% w/w aq), tetra-n-propylammonium hydroxide (TPAOH, 40% w/w aq.), and benzyltrimethylammonium hydroxide (BTMAOH, 25% w/w aq.) all from Alfa Aesar. Electrochemical measurements were made using an Autolab Potentiostat/Galvanostat Model PGSTAT30 (Metrohm USA).

The electrochemical behavior of the transition metal complexes were studied at an alkaline ionomer modified glassy carbon electrode. A glassy carbon rotating disk electrode (Ageo = 0.247 cm2), after polishing and pretreatments described above, was allowed to dry after deposition of 5 μL of 5 wt.% anion exchange ionomer (Tokuyama AS4) on the surface. The electrode was placed in an argon saturated 0.1 M NaOH solution and subjected to 20 cycles from 0.05 V to 1.2 V at 50 mV/s and five cycles at 20 mV/s. 10 mM of K3Fe(CN)6 was then added to the solution and the solution was purged with argon for an addition 10 minutes before collecting data. This experiment was repeated using 10 mM $Co(NH3)_6Cl_3$ in place of $K_3Fe(CN)_6$.

The focus of this study is on the low electrode performance in direct alcohol, AEM fuel cells, compared to Nafion®-based PEM cells. The addition of alkali metal hydroxide improves the cell performance, but the results are less than optimal. It should be emphasized that the addition of excess KOH in the anode feed is highly undesirable given the alkali metal carbonate precipitation issues. [1]

Results and Discussion:

The performance of a direct ethanol alkaline fuel cell was characterized with and without the presence of excess KOH in the anode fuel. Figure 4 shows the polarization and power density

curves for an AEM fuel cell with an anode composed of 4.0 mg_{PtRu}/cm^2 + 1.0 mg_{AS4}, cathode composed of 30% Pt/C (1.0 mg_{Pt}/cm^2 + 28 wt.% AS4) + 1.0 mg_{AS4}, and Tokuyama A201 anion exchange membrane. The cell was first operated with 1 M EtOH anode feed, which was later changed to 1 M EtOH with 0.25 M KOH. The results shown in Figure 4 are typical of all prior reports wherein there is a low open circuit potential (OCP), severe drop in potential at low current density and low power density when operated in the absence of KOH. The OCP improved from 0.68 V to 0.85 V when KOH was added to the anode feed. In the absence of KOH the maximum power density was 1.7 mW cm^{-2} at 5 mA cm^{-2} and 0.335 V. The maximum power density improved to 22.4 mW cm^{-2} at 64 mA cm^{-2} and 0.350 V when KOH was added to the fuel. For comparison, Liang et al [2] reported 23 mW cm^{-2} using 1 M EtOH with 1 M KOH anode feed and pure O_2 at 50°C with a Tokuyama A201 membrane, 2.0 mg cm^{-2} HYPERMEC™ anode catalyst loading and 1.0 mg cm^{-2} HYPERMEC™ cathode catalyst loading. Fujiwara et al. [3] achieved a power density of 58 mW cm^{-2} using 3.0 mg_{PtRu} cm^{-2} with 5 wt.% anion exchange resin at the anode and a Tokuyama AEM when 1.0 M EtOH with 0.5 M KOH was used as the fuel. Only 8 mW cm^{-2} was obtained in the absence of KOH. Additionally, Hou et al [4] reported power densities of ~50 and ~60 mW cm^{-2} at 75°C and 90°C, respectively for a cell consisting of alkali metal hydroxide doped PBI membrane with 2.0 mg_{PtRu} cm^{-2} anode and 1.0 mg_{Pt} cm^{-2} loadings at the anode and cathode, respectively operating on 2 M EtOH in 2 M KOH anode feed. It should be noted that in each of the aforementioned studies [2-4], a sharp drop in cell potential occurred at very low current densities followed by modest drop in cell potential as the current reached the mass transfer limited regime. In addition, the steep decline in potential at low cell current has also been observed in all fuel cells operating with methanol fuel supply [5-8] as well as studies with other alcohols [5-7]. These results indicate that the overall performance suffers significant cell voltage loss at low currents regardless of the choice of fuel. Moreover, the steep drop in potential has been observed for several different catalysts, including Pt/C [5, 9], Pt/Ti [8], and PtRu [7].

Figure 5 shows the AC impedance spectra of the fuel cell corresponding to Figure 4 taken with and without excess KOH in the anode feed. By plotting the imaginary versus real components of impedance, the charge transfer resistance, R_{CT}, was obtained after fitting the data to a semicircular curve and determining the difference between the high frequency and low frequency intercepts on the real axis. Similarly, the ionic resistance (R_{ionic}) of the membrane was determined from the x-intercept at the high frequency. It should be noted that the semicircular shape of the plot is indicative of the kinetically controlled region, while the absence of Warburg impedance, for the given potential and frequency range, suggests that the process is not diffusion controlled. When the cell was operated in the absence of KOH, it was found that R_{CT} and R_{ionic} were 84.25 and 2.95 Ω cm^2 , respectively. The values obtained for the cell operated in the presence of KOH was R_{CT} = 6.55 Ω cm^2 ohm, and R_{ionic} = 0.55 Ω cm^2, which are significantly lower. The lower values of R_{CT} found in the presence of KOH indicate that the ethanol oxidation kinetics were dramatically improved with the addition of KOH. A modest drop in R_{ionic} is expected in the presence of KOH since it increases the ionic conductivity of the membrane and the interface. The lower values for R_{CT} suggest that the rate of ethanol oxidation increased markedly with addition of KOH.

It is important to understand the source of performance loss in the absence of added KOH for each of the cell components. Typically, alkaline membrane fuel cells operating with H_2/O_2 achieve more than 500 mA cm^{-2} with similar cathode structures. Also, since the addition of KOH

to the anode liquid fuel dramatically changes the AC impedance, it is reasonable to conclude that the performance of current alkaline alcohol fuel cells is primarily limited by anode performance. Further analysis of the alcohol oxidation anode was performed with an alcohol/H_2 half-cell system. Figure 6 shows the half-cell ethanol oxidation profile obtained from a cell operating with a 2.0 mg_{Pt}/cm^2 anode and the same cathode and membrane as described for the cell used in Figure 4. Humidified H_2 was used at the cathode which also served as the reference electrode. The maximum current density obtained for ethanol oxidation at 0.8 V was 5.7 mA cm^{-2} and 89.7 mA cm^{-2} in the absence and presence of 0.25 M KOH, respectively. Here, it can be seen that the rate of ethanol oxidation is significantly enhanced with excess KOH. No clear onset potential for ethanol oxidation could be discerned in Figure 6 when in the absence of KOH from the anode feed. This half-cell result shows that the anodic oxidation of alcohol in the absence of excess KOH is a major limiting factor in the performance of alkaline direct alcohol fuel cells. Then, the percent loss in current density after 900 sec potential control at 600 mV (vs. RHE) in 0.1 M KOH was recorded as a function of quaternary ammonium as shown in Figure 7. In general, all ammonium cations showed a significant adsorption effect on the platinum surface resulting in loss of methanol oxidation activity. The decrease in current became more pronounced at higher concentrations of the added cations. TMA+ showed the smallest drop in current, whereas the other three cations with bulkier substitute groups resulted in substantially greater loss in current. This observation is consistent with previous literature that showed a higher surface inhibition with the longer alkyl length on the ammonium group. [48]

These results with different quaternary ammonium cations in aqueous electrolytes show that quaternary ammonium ion adsorption on Pt surfaces lowers the rate of methanol oxidation by blockage of the active catalyst surface area. However, the solid polymer electrolyte, ion-conducting medium in a polymer-based fuel cell is different from that of free ions in an aqueous solution. A fuel cell electrode consists of quaternary ammonium cations with little chain segment mobility tethered to a polymer backbone. Figure 8 displays the cyclic voltammograms for the Fe(CN)63-/4- redox couple on a GC electrode with and without a deposited film of AS4 ionomer. Typically, the current magnitude cannot be used to make a direct comparison between solution and AEM environment because both concentration and diffusion coefficients changes. However, the difference between the oxidation and reduction peaks can be evaluated to define a change in reaction rates. From Fig. 8, it can be seen that the peak separation (ΔEp) decreases from 279.5 mV in the absence of AS4 to 131.0 mV in presence of the AS4 ionomer film. In contrast, Figure 9 shows the CV profiles for the $Co(NH3)_6^{2+/3+}$ redox couple on a GC electrode with and without a deposited film of AS4 ionomer. The current densities are lower with AS4 ionomer than without ionomer because AS4 ionomer mostly excludes positively charged species, decreasing the concentration on the electrode surface, i.e. lower current. However, it is critical to note that there is a slight increase in ΔEp from 65.3 mV to 83.9 mV in the presence of ionomer.

For these redox couples, the electrode potentials are more positive than PZC, ca. -0.1V, at the electron transfer potentials and the reaction occurs through an outer-sphere electron transfer pathway. The double layer structure differs from the methanol oxidation region where the electrode potential is more negative than PZC. Figure 10 shows the double layer structure when the electrode potential is greater than PZC in the presence and absence of AEM ionomer. As a distinct difference, the diffuse layer in an AEM becomes thicker relative to in the absence of an AEM. Consequently, f2 is more positive in the presence of AEM. For negatively charged redox couple, both exponential terms favor the electron transfer, i.e. higher kinetics. This is consistent

with the lower peak splitting for $Fe(CN)_6^{3-/4-}$ in Figure 8. However, for positively charged species, the driving force still favors the reaction but the transport of these species is inhibited. This inhibition factor is greater than the enhancement in driving force, resulting in lower reaction kinetics. This is consistent with the greater peak splitting in Figure 10.

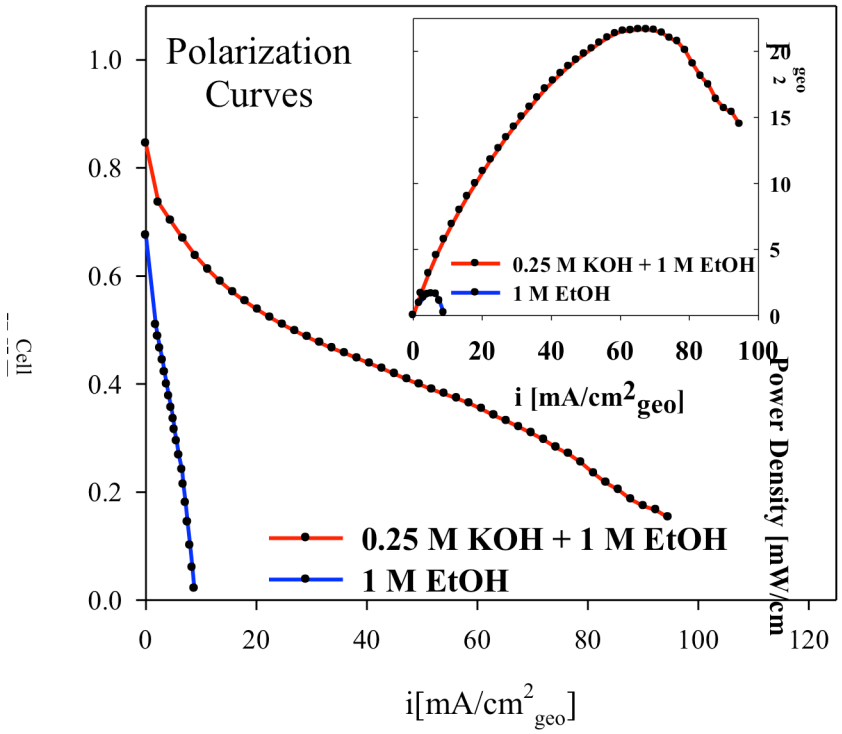

Figure 4. - Direct ethanol fuel cell polarization curves taken at 50°C. Anode: PtRu on Toray paper (Loading = 4.0 mgPt/cm2) with 1 mgAS4/cm2 interfacial ionomer film on surface. Cathode: 30% Pt/C on GDL (Loading = 1 mgPt/cm2 + 28.5 wt% AS4 ionomer) with 1 mgAS4/cm2 interfacial film on surface. Tokuyama A-201 membrane. Anode feed: 1 M EtOH with/without 0.25 M KOH at 8 mL/min. Cathode feed: 100 % RH O2. Inset shows the corresponding power density curves.

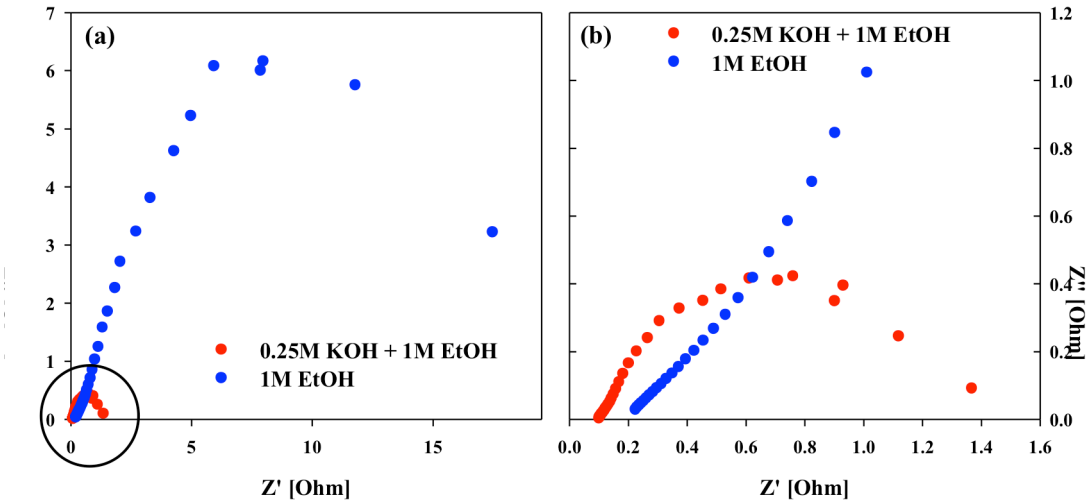

Figure 5. (a) Impedance spectra at 50°C collected at 0.4 V from 20 kHz to 0.1 mHz with an amplitude of 0.05 V. AEM fuel cell configuration same as that in Figure 1. Anode feed: 1 M EtOH with/without 0.25M KOH at 8mL/min. Cathode feed: 100% RH O2. (b) Magnified plot of the circled region in (a)

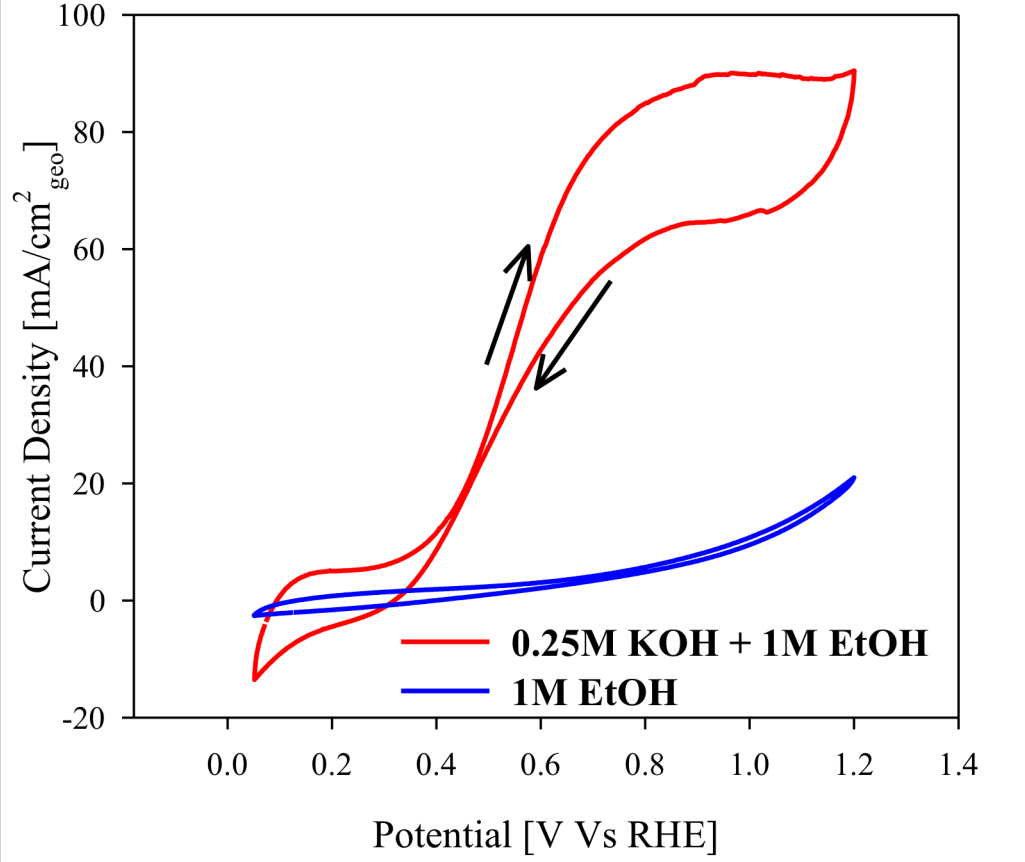

Figure 6. Ethanol oxidation curve at 50°C. Scan rate: 20 mV/s. Anode: Pt on Toray paper (Loading = 2.0 mgPt/cm2) with 1mgAS4/cm2 ionomer film on surface. Cathode: 30% Pt/C on GDL (Loading = 1 mgPt/cm2 + 28.5 wt.% AS4 ionomer) with 1mgAS4/cm2 ionomer film on surface. Tokuyama A-201 membrane. Anode feed: 1M EtOH with/without 0.25M KOH at 8mL/min. Cathode feed: O2 100% RH

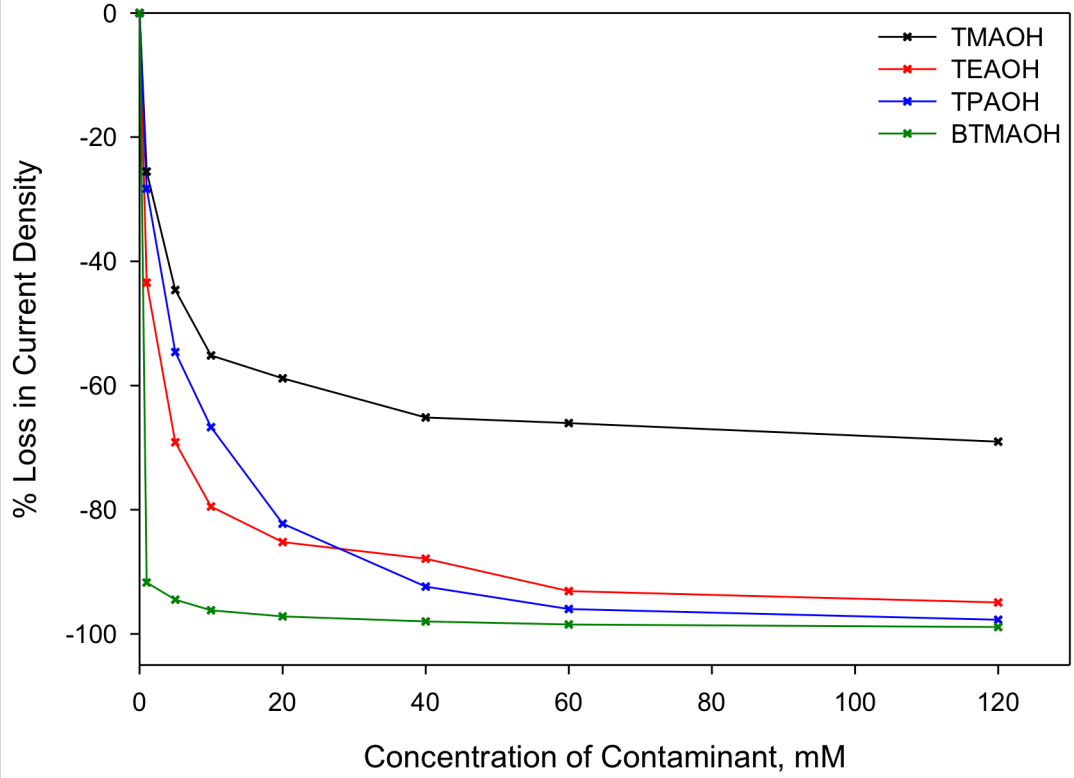

Figure 7. Percent loss in current density as a function of contaminant concentration in 0.1M KOH + 0.5M MeOH + x mM contaminant. Glassy carbon disk electrode (0.247 cm2) with 5 µL of 30% Pt/C ink deposited (Loading = 7.5 ugPt/cm2). Steady state currents obtained from chronoamperometry at 0.6V vs RHE at 900 seconds.

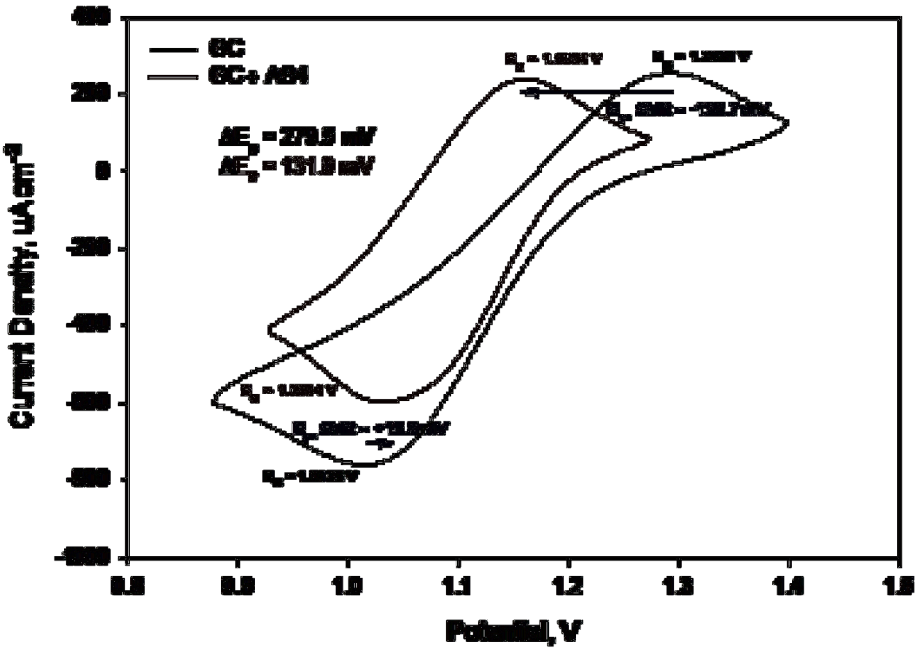

Figure 8. CV of Fe(CN)63-/4- redox couple in Ar saturated 0.1M NaOH + 10mM K3Fe(CN)6 solution. Scans performed on glassy carbon disk electrode with 5 µL of 5 wt.% AS4 ionomer deposited on surface. Geometric surface area = 0.247 cm2. Scan rate = 20 mV/s

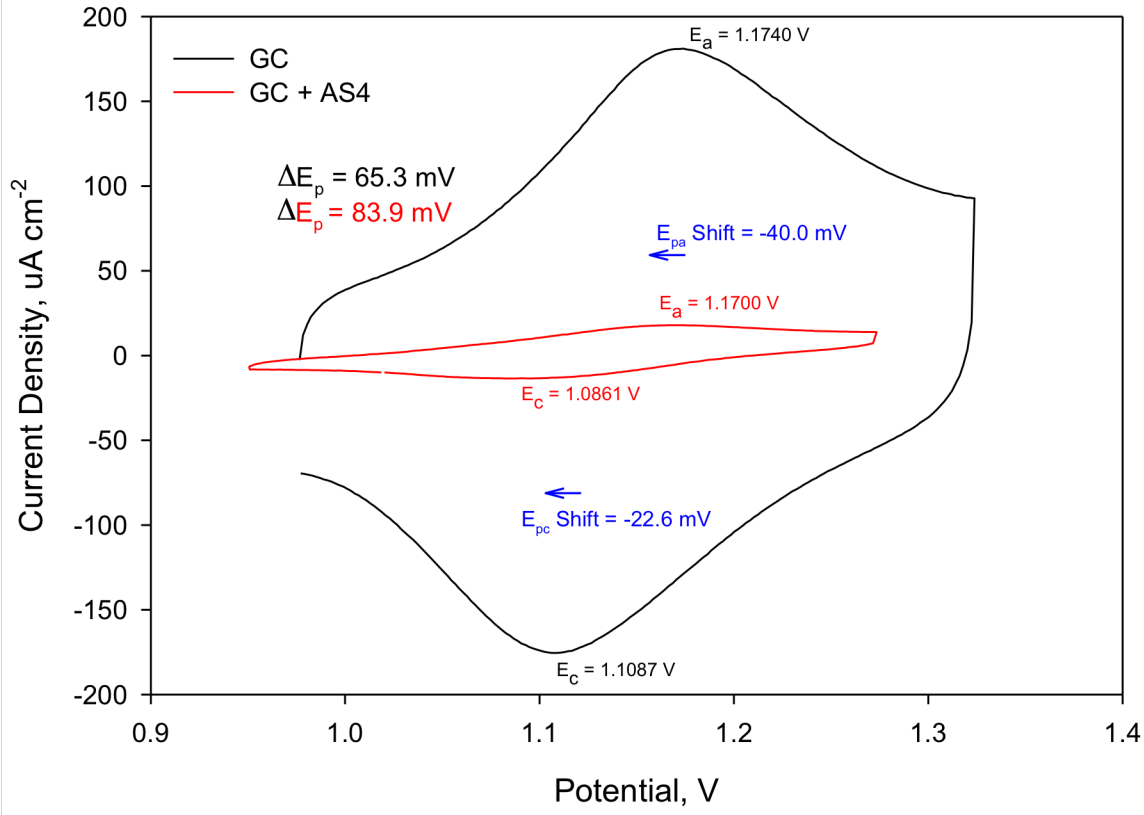

Figure 9. CV of Co(NH3)62+/3+ redox couple in Ar saturated 0.1M NaOH + 10mM Co(NH3)6Cl3 solution. Scans performed on glassy carbon disk electrode with 5 µL of 5 wt.% AS4 ionomer deposited. Geometric surface area = 0.247 cm2. Scan rate = 20 mV/s

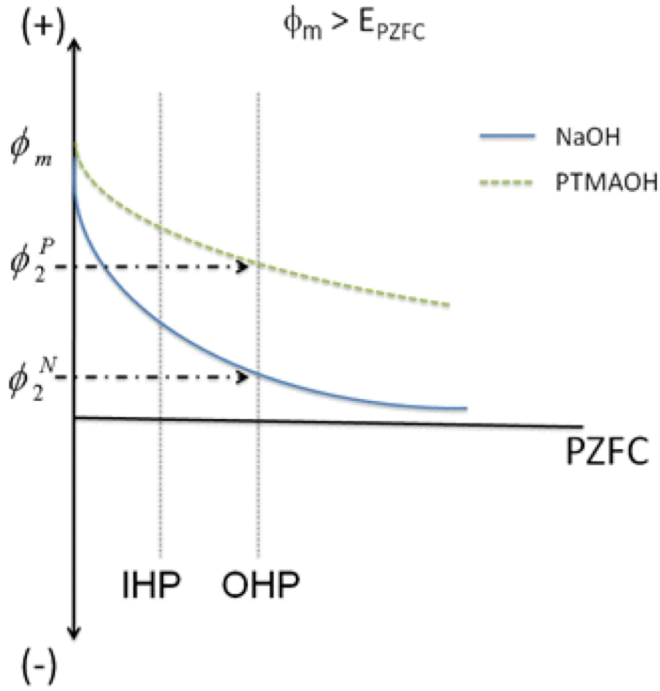

Figure 10. Expected potential profile of anode double layer interface in the presence and absence of anion exchange ionomer when the electrode potential is more positive than

Activity Descriptor Identification for Oxygen Reduction on Non-Precious Electrocatalysts: Linking Surface Science to Coordination Chemistry

Published Articles:

1. 'Fundamental Mechanistic Understanding of Electrocatalysis of Oxygen Reduction on Pt and Non Pt Surfaces: Acid vs. Alkaline Medium', N. Ramaswamy and S. Mukerjee, *Advances in Physical Chemistry*, **Vol. 2012**, Article ID 491604, (2012).
2. 'Activity Descriptor Identification for Oxygen Reduction on Non-Precious Electrocatalysts: Linking Surface Science to Coordination Chemistry' Nagappan Ramaswamy, Urszula Tylus, Qingying Jia and Sanjeev Mukerjee, *JACS* **135 (41)**, 15443 (2013).

The drive to replace expensive precious-metal-group (PGM) systems for ORR has led to a class of catalysts comprising transition metal-ions stabilized by nitrogen functional groups on carbonaceous surfaces (Fe-N_x/C)[10-12]. These active sites are adventitiously synthesized via pyrolysis of precursors containing transition metals, nitrogen, and carbon, all of them either present in the same source or different sources[13]. Potential multiplicity of active sites for initial O_2 adsorption and the lack of suitable analytical techniques complicates a lucid understanding of the nature of active sites and the reaction mechanisms in these composite catalysts[11]. Despite high activity and durability of pyrolyzed Fe-N_x/C catalysts shown recently[14-16], current progress primarily involves an experiential approach of trial-and-error combination of precursors and pyrolysis conditions to maximize performance. Lack of fundamental understanding of the mechanistic origin of ORR and the underlying surface material properties that govern catalytic activity clearly limits further progress. Here, for the first time we present a direct structure-activity relationship between the intrinsic ORR turnover number (i.e. kinetic current-density normalized by electrochemically active site-density quantified via square-wave voltammetry) and a surface material property of pyrolyzed Fe-N_x/C catalyst; thus, providing deep insight into the fundamental mechanistic origin of ORR and potentially opening the door to elegant bottom-up catalyst synthesis strategies.

Electrocatalysis on *non-pyrolyzed* metal-macrocycles is governed by the nature of the i) central metal-ion and ii) the surrounding macrocyclic ligand[17]. While d-electron density on the metal-ion determines the progress of ORR via adsorbed intermediates, the role of π-conjugated ligand is to modify the metal-ion's electronic structure by relocating its redox potential[17, 18]. Based on molecular-orbital approach, end-on M-O_2 interaction primarily involves σ-type bonding between O_2 molecular orbitals and e_g-orbital (d_z^2) of the transition metal-ion.[17, 19-21] Further in accordance to the redox mechanism,[22, 23] ORR onset potential is closely linked to the metal-ion's redox potential which in turn essentially represents the e_g-orbital (d_z^2) energy level.[24] Thus, a downshift in energy level of e_g-orbitals away from the Fermi level anodically shifts the metal-ion's redox potential leading to higher ORR onset potentials, and optimizes the adsorption strength of ORR intermediates leading to higher turnover numbers. Downshift of e_g-orbitals is possible via i) substitution of electron-withdrawing groups on the macrocycle ring,[25, 26] and/or ii) formation of electron donor-acceptor pair between metal-macrocycle and carbon basal plane via π-π interaction (due to electron-withdrawing nature of de-localized π-electrons in carbon basal plane relative to π-electron rich macrocycle).[27] However, both these routes

involve long-range non-covalent interactive forces leading to a minor potential shift (~ 200 mV), insufficient to cause significant change in ORR onset potential.

Here, we show that the pyrolysis step covalently integrates the Fe-N_x active site into the π-conjugated carbon basal-plane, causing a dramatic anodic shift of ~600-900 mV in the metal-ion's redox potential. Since the carbon basal-plane constitutes an intricate integral part of the active site rather than merely an electrically conducting high surface area support, the surface chemistry of underlying carbon needs due consideration[28-30]. We show that the electron-donating/withdrawing capability of the carbon support, conferred upon it by the de-localized π-electrons, acts as a primary activity descriptor that governs ORR electrocatalysis on pyrolyzed Fe-N_x/C active-sites. In addition, we also elucidate the aspect of outer-sphere electron transfer mechanism during ORR in alkaline media; particularly in light of recent evidences highlighting the necessity to promote inner-sphere electron transfer mechanism via direct chemisorption of de-solvated O_2 on the active-site.[31-33] Using iron(III) meso-tetraphenylporphine chloride (FeTPPCl) as a model system, we elucidate inner- vs outer-sphere ORR mechanisms, active-site structure evolution and most importantly, establish scientifically relevant electrocatalytic activity trends to provide a fundamental molecular level understanding of ORR on pyrolyzed Fe-N_x/C catalysts.

In this work, we have developed scientifically relevant fundamental molecular-level understanding of ORR on pyrolyzed Fe-N_4/C catalysts. The Lewis basic nature of carbon basal-plane facilitates the formation Fe-N_4 active sites on carbonaceous surfaces via the nitrogen coordinating atoms. The pyrolysis step adventititously relocates the Fe-N_4 active site from a π-electron rich macrocyclic ligand environment to a relatively π-electron deficient graphitic carbon environment. Divacant defective pockets and the edge-plane sites appear to provide such a π-electron deficient environment in the carbon support; this causes a significant modification in the electron density and energy level of the e_g-orbital (d_z^2) of the transition metal-ion leading to a significant anodic shift in its redox potential. Further, the degree of π-electron de-localization on disordered graphitic carbon basal planes can be used as a parameter to modulate the adsorption strength of ORR intermediates and the intermolecular hardness of the adducts. On biomimetic active-sites, the operation of redox mechanism ensures direct O_2 adsorption on the Fe^{2+}-N_4 active site and prevents the outer-sphere reaction of solvated O_2 with the OH_{ad}-covered active site. A unified picture is developed here by combining the principles of surface science and coordination chemistry, wherein the concepts of Sabatier's principle and intermolelar hardness are utilized to comprehensively expound the fundamental molecular level understanding of ORR on Fe-N_4/C catalysts. A unique feature of the class of pyrolyzed catalyst is the ability to tune the catalytic activity by experimentally controlling the degree of π-electron de-localization of the carbonaceous surfaces. This phenomenon will likely open the door to the development of more active and stable electrocatalysts based on biomimetic active-sites on novel π-surfaces.

Some of the representative figures and tables which define the above mentioned conclusions are provided below:

Figure 11: ORR activity and mechanisms on pyrolyzed non-precious metal catalysts. (a) Schematic illustration of inner-sphere (inset i) and outer-sphere (inset ii) electron transfer mechanisms during ORR in alkaline media. (IHP - Inner Helmholtz Plane, OHP - Outer Helmholtz Plane). Comparison of the electrochemical characteristics of Fe-N_x/C catalyst (pyrolyzed at 800°C) in O_2-saturated 0.1 M $HClO_4$ and 0.1 M NaOH electrolytes showing (b) ORR activity (i_D) and concomitant ring-current (I_R) due to hydrogen peroxide oxidation. Also shown for comparison in (b) is the ring current profile measured during ORR on Pt/C catalyst deposited on the disk-electrode. (c) Hydrogen peroxide reduction reaction (HRR) activity in argon-saturated electrolytes containing 3.5 mM H_2O_2 in comparison to ORR. HRR experiments were carried out by scanning the potential in the cathodic direction starting from the open-circuit potential so that any influence due to O_2 evolved from H_2O_2 electro-oxidation is avoided. Scan rate - 20 mV/s, rotation rate - 900 rpm, E_{Ring} = 1.1 V vs. RHE in 0.1 M NaOH and 1.3 V vs. RHE in 0.1 M $HClO_4$, Fe-N_x/C loading - 100 μg/cm^2, Pt/C loading - 15 μg_{Pt}/cm^2 on 5.61mm Glassy Carbon disk at 900 rpm.

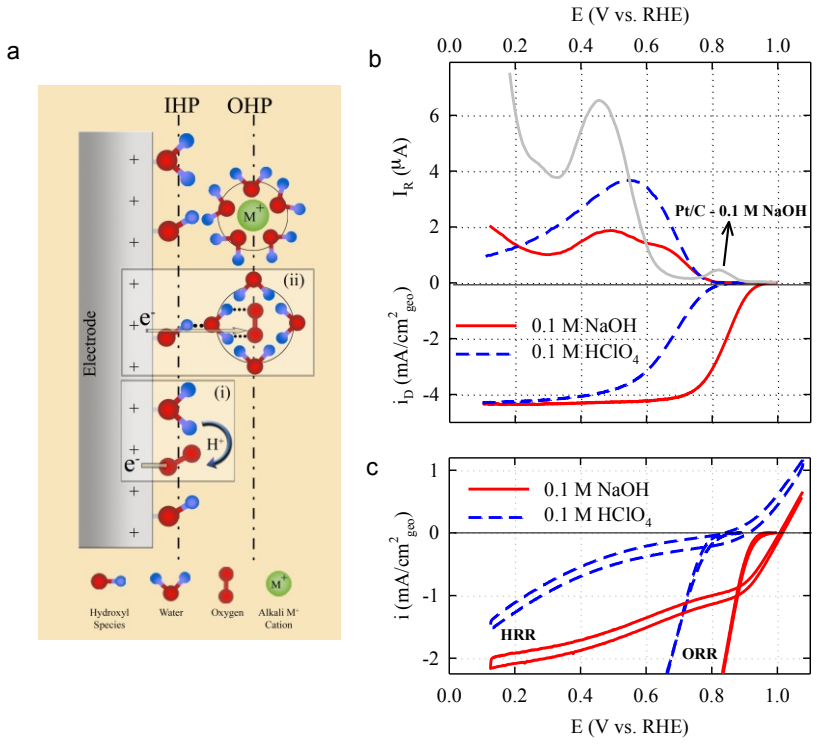

Figure 12: Active site structure identification. Experimental XANES and delta-mu signatures of Fe-N_x/C catalyst pyrolyzed at (a) 300 °C and (c) 800 °C. delta-mu signatures were obtained by subtracting the XANES signatures according to $\Delta\mu = \mu(0.90 \text{ (or) } 1.10 \text{ V}) - \mu(0.10 \text{ V})$. Experiments were conducted at Fe K-edge under *in situ* conditions in argon saturated 0.1 M NaOH electrolyte. Vertical dotted line indicates the pre-edge position at 7112.5 eV. Structural models shown in the inset of (a&c) were utilized for delta-mu analysis using FEFF8 simulation. Also shown are the complete structural models of active site structures before (b) and after (d) pyrolysis at 800 °C. Color Codes in structural models: Red – iron; Blue – nitrogen; Gray – carbon and White - oxygen.

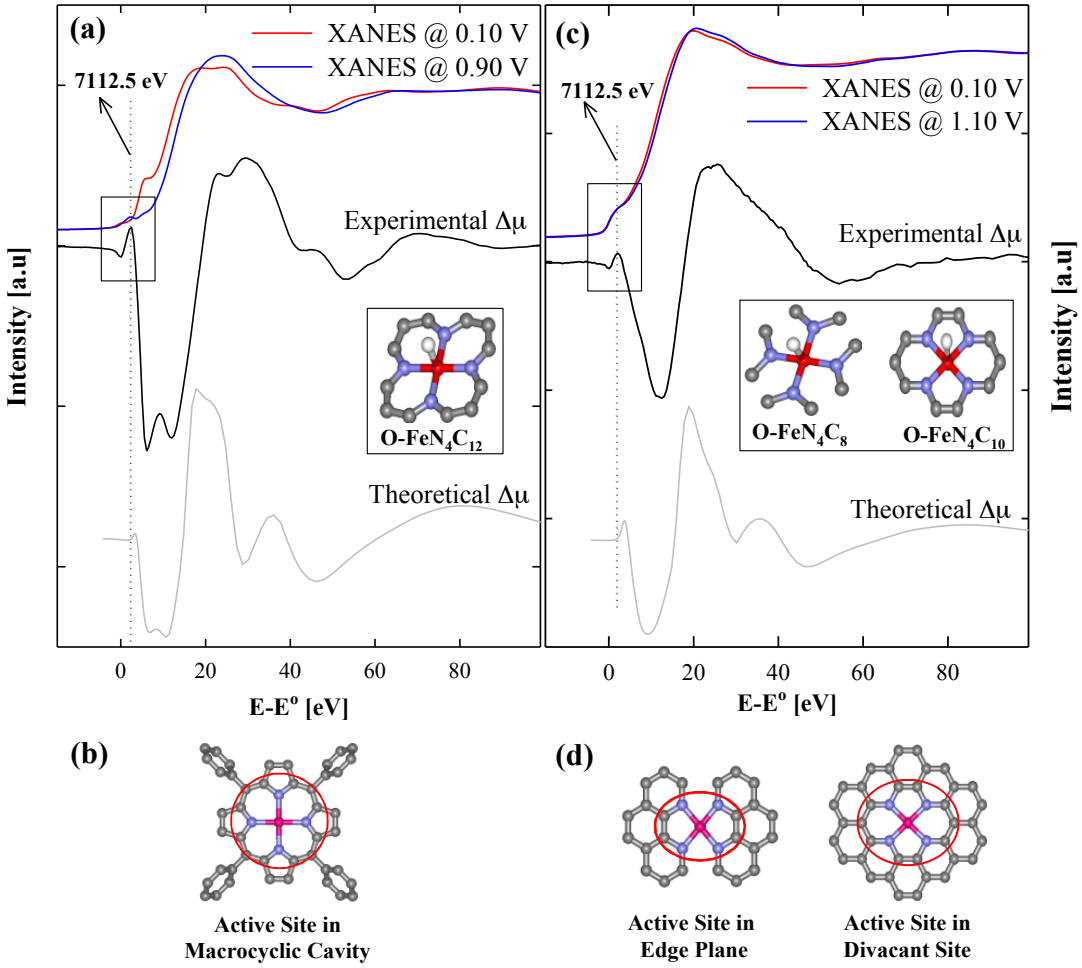

Figure 13: Redox potential of active site. (a) Square wave voltammetry (SWV) profiles of Fe-N_x catalyst supported on black pearl carbon before and after pyrolysis at 800 °C in 0.1 M $HClO_4$ and 0.1 M NaOH electrolytes. (b) Plot showing the effect of pyrolysis temperature on Fe-N_x/C redox peak potential (E_P) in 0.1 M NaOH and full-width at half-maxima of C1s photoemission spectra. SWV profiles after pyrolysis have been multiplied by a factor of 7 for visual comparison.

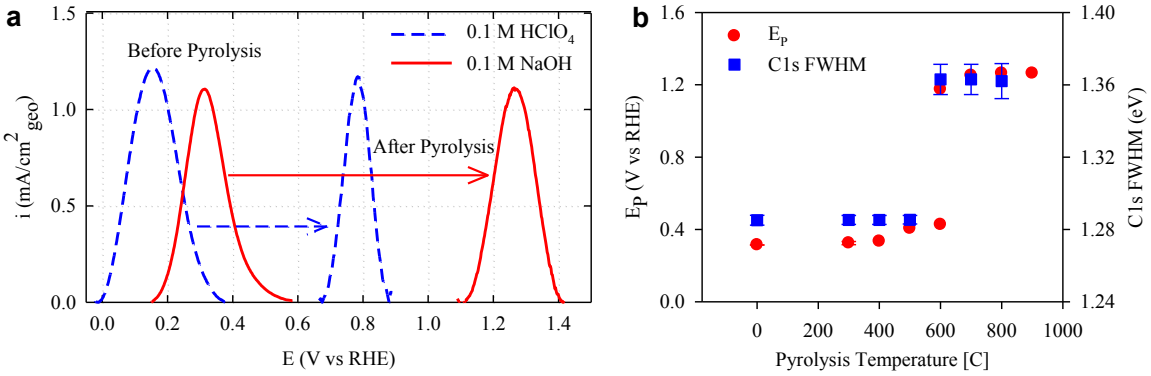

Figure 14: Relationship between ORR turnover number and electron-withdrawing character of carbon basal plane. (a) ORR activity of Fe-N_x/C catalyst (pyrolyzed at 800 °C) on various carbon supports in O_2-saturated 0.1 M NaOH electrolyte at 900 rpm rotation rate and 20 mV s^{-1} scan rate. (b) Linear relationship between ORR turnover numbers in 0.1 M NaOH electrolyte versus full-width at half maximum of C1s photoemission spectra. (c) Schematic illustration of intermolecular hardness (η_{DA}) parameter in Fe^{2+}-O_2 or alternatively Fe^{3+}-(O_2^-) adducts.

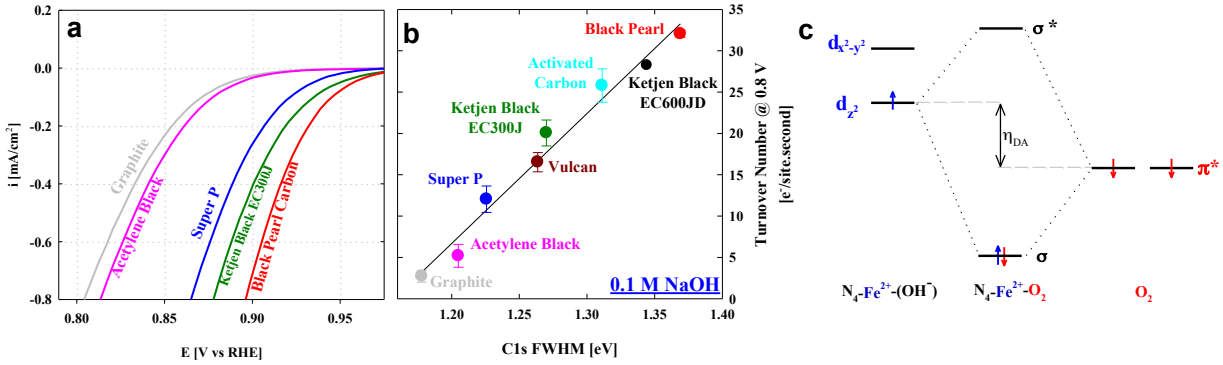

Figure 15: Proposed ORR Mechanism. Catalyst cycle showing the redox mechanism involved in ORR on pyrolyzed Fe-N_x/C active sites in dilute alkaline medium.

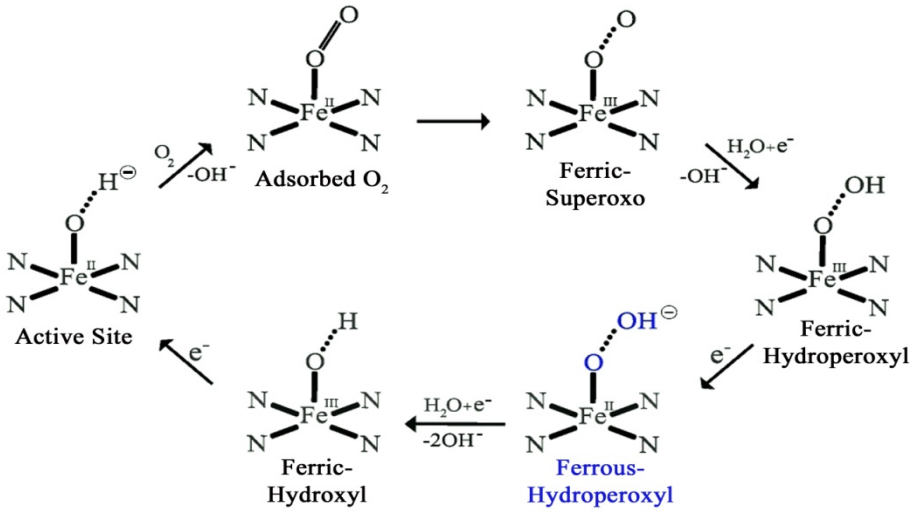

Dramatically Enhanced Cleavage of the C-C Bond Using an Electrocatalytically Coupled Reaction

Published Article: Dramatically Enhanced Cleavage of the C-C Bond Using an Electrocatalytically Coupled Reaction' Q. He, B. Shyam, K. Macounova, P. Krtil, D. Ramaker, S. Mukerjee,**JACS*, 134, (20) pp 8655-8661 (2012).

The controlled electrocatalytic cleavage of the C-C bond in organic molecules, particularly in aliphatic alcohols, remains one of the most challenging problems in electrochemistry. Aside from a fundamental interest in directing a multi-electron transfer to selectively cleave or form C-C bonds,[34] the reaction is also of great practical significance in the development of fuel cell-based electric energy generators.[35, 36] This implementation enabling higher alcohol oxidation can significantly improve the energy density of these low-temperature fuel cells. The inertness of the C-C bonds in electrocatalytic alcohol oxidation is counterintuitive, since the C-C bonds are relatively weak and can be, in the case of hydrocarbons, cracked either thermally or catalytically.[37] Taking ethanol as an example, a cleavage of the C-C bond in the oxidation process leading eventually to CO2 formation (12 electrons) is severely disfavored kinetically, especially in acid media.[38] The electrocatalytic oxidation of aliphatic alcohols proceeds readily on Pt based metal surfaces but usually yields just 2 to 4 electrons per alcohol molecule, and depending on both the electrode material and the pH, rarely involves C-C bond splitting.[39-41] The resulting products are mostly the undesired aldehydes or corresponding acids at low pH. In contrast, in alkaline media more complete oxidation occurs, mainly due to higher sensitivity to structural and morphological moieties such as relative population of crystallite planes.[42, 43] Ethanol oxidation, selective to CO2, has been reported for Pt polarized to potentials in the oxygen evolution region in alkaline media.[44] The oxidation process is, however, far from controlled at these conditions.

Regardless of the media, Pt based materials represent the benchmark catalysts for ethanol oxidation. There have been several strategies devised for enhancing the activity and selectivity of electrocatalytic ethanol oxidation,[45-48] some based on incorporation of ad-atoms to the surface. The enhancement has been attributed to steric hindrance of the surface, or electronic ligand and/or bi-functional effects when the ad-atoms are directly involved in the catalytic process.[49] The activity of purely metal based catalytic systems is reported to be surpassed by multifunctional catalysts featuring metal oxide based oxidation promoters like, e.g. MgO,[50] CeO2,[51] ZrO2,[52] or SnOx.[40, 53] Despite the apparent improvement of the activity in the ethanol oxidation, the resulting selectivity of the oxidation process towards the desired 12 electron process still significantly lags behind expectations, with a gradual deactivation of the catalyst surface in the course of minutes. The rationalization for the C-C bond inactivity in ethanol oxidation arises because the ethanol molecule primarily adsorbs to the metal surface via the oxygen on the C1 carbon. The first electron removed from the ethanol molecule facilitates formation of the energetically more stable aldehyde, which then easily desorbs from the surface preventing further charge transfer that could attack the ethanol C-C bond.[54, 55] It may be envisaged that controlling the approach, and hence the adsorption mode of ethanol, toward the substrate could be instrumental in steering the selectivity of the oxidation process towards the C-C bond splitting essential for the complete oxidation route.

The part of the effort showed for the first time the successful application of this concept, utilizing a solution-based co-catalyst to direct the ethanol adsorption, while modifying the catalyst surface chemistry to oxidize selectively the C-C bond in ethanol. Differential electrochemical mass spectroscopic (DEMS) and in-situ X-ray absorption near-edge spectroscopy (XANES) data were used to show and rationalize the behavior of the Pb (IV) acetate under reaction conditions, thus modifying the behavior of the Pt/C nanoparticulate catalyst to retain an unprecedented activity and selectivity towards C-C bond breaking on the timescale of hours.

Combination of electrochemical and spectrometric data shows for the first time an effective strategy for combining homogeneous and heterogeneous processes directing both the activity as well as the selectivity of electrocatalytic oxidations of organic molecules, specifically involving cleavage of the C-C bond.

A cathodic shift of 150 mV of the onset potential for ethanol oxidation was observed on a Pt/C electrode in the presence of 1mM Pb(IV). Chronoamperometric measurements reveal that a steady state current remains 1 hour later (up to 56% of the initial), and is higher than any reported to date. The lead ions were found to play a dual role in the catalysis: Pb(OH)2 is adsorbed on the Pt surface and produces OH adsorption at lower potentials to oxidize the CO and other carbonyl species, and Pb(II) and/or Pb(IV) ions form a complex with ethanol before it reaches the electrode surface, which appears to be beneficial for the C-C bond breakage either by influencing the orientation of the ethanol as it approaches the surface or even by assisting in the bond breaking directly. The excellent sustained activity shown in the case of ethanol oxidation accompanied with high selectivity to complete oxidation outlines the potential of this strategy for use in electrocatalytic power generating applications.

Included below is the summary of this effort in terms of the overall mechanism of activity enhancement (figure 16).

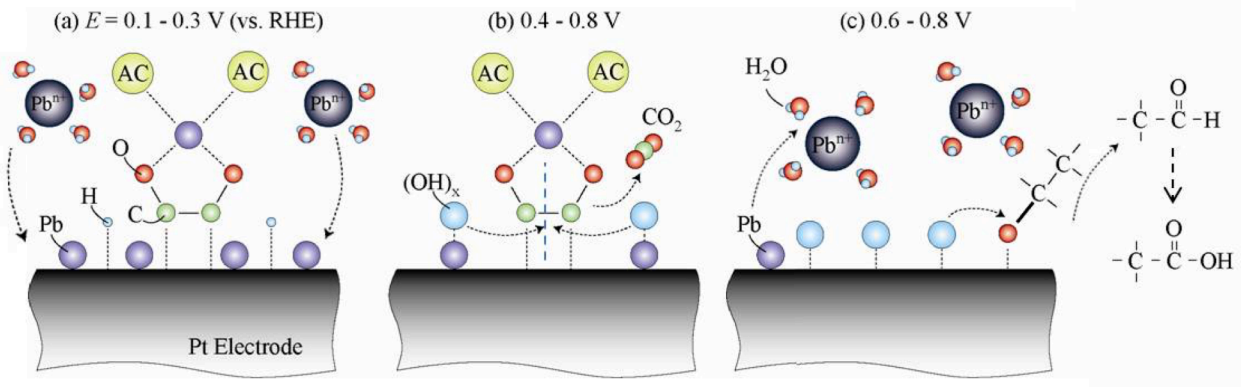

Figure 16. Working mechanism of electrooxidation of ethanol on the Pt electrode with the assistance of Pb acetate at different potentials in alkaline media

Harvesting Hot Electrons of Plasmonic Nanostructures for Efficient Photocatalytic and Electrochemical Reactions

BACKGROUND To solve the global energy crisis, renewable energy sources, especially solar energy, have attracted intensive interest in industry and academia. Photocatalysis promises to be an exciting method for harvesting solar energy and thereby promoting the sustainable energy needs of society. One benchmark example of photocatalytic reactions is water splitting, in which electrons and holes diffuse to the surface of the semiconducting material and promote the dissociation of water to form H_2, O_2, and OH^- radicals.[56-58] The vast majority of research in this domain has focused on the interaction of photons with semiconductor TiO_2 largely due to its ability to directly transfer photon energy into highly reactive chemical species and relatively low cost.[59] However, its drawbacks (and those of similar materials) include (1) the requisite wide band gap (approximately 3 eV) and the resulting limitation of photon absorption to a narrow band within the UV range, (2) the requirement for high surface area to achieve maximum catalytic efficiency, and (3) the need to minimize charge recombination by the imposition of various structural features. **In this program, we aim to significantly improve the efficiency of photocatalysis by directly harvesting the hot electrons when the plasmonic resonance of metallic nanostructures is excited. Moreover, we will explore the possibility of steering hot electrons to participate in electrochemical reactions, which would open a new horizon in the field of solar-chemical energy conversion.** Light absorbed by a metal can produce photo-excited hot carriers. At the surface plasmon resonant frequency, the collective electron oscillation leads to enhanced light absorption and hence more hot carriers can be generated. These carriers transport over distances of a few tens of nanometers to the interface of the metal, and eventually could be injected into neighboring semiconductor active materials, or electrolyte. The hot carriers can drive various chemical reactions, such as, dissociation of H_2,[60] or the oxidation and reduction reactions that evolve O_2 and H_2 from water.[61] We plan to use rationally designed and fabricated plasmonic nanostructures to enhance photon absorption over a broad wavelength range for hot carrier excitation and efficient solar-chemical energy conversion.

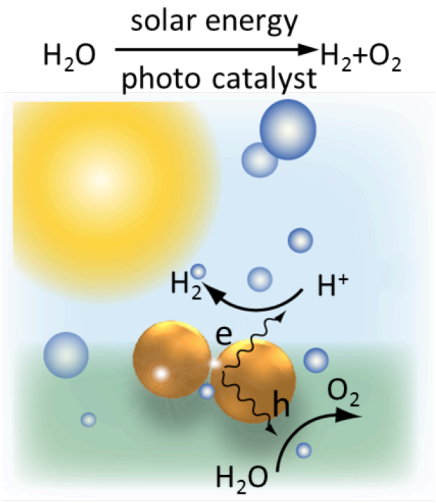

Figure. 17. Schematic of water splitting, and the proposed work of using the hot electrons of plasmonic nanostructures (gold color) to significantly enhance solar energy

PROJECT DESCRIPTION We are in the process of using rationally designed and fabricated plasmonic nano-structures to enhance photon absorption, leading to a potentially new paradigm in photocatalysis. Different from traditional heterogeneous photocatalysts (principally semiconductors), the use of metallic plasmonic structures should significantly improve efficiency. Extending prior work,[62, 63] we will explore how photons and plasmons facilitate carrier excitation and transport at the deep sub-wavelength scale, and how they regulate photochemical reactions for hydrogen, oxygen generation.

Plasmonics Assisted Broadband Absorption Photon absorption should ideally be broadband and efficient in order to absorb over the entire solar spectrum. Metallic (plasmonic) nanoparticles can resonantly enhance light absorption due to the excitation of plasmonic modes. Moreover, the absorbance spectral position can be tuned by changing the size, geometry and materials properties of such structures. Both the near-field field enhancement and far-field scattering effect contribute to absorbance enhancement in active materials. However, the absorption bandwidth is limited to about 100 nm in the visible regime for simple plasmonic nanostructures, due to the low quality factor of the electric dipole resonance. Although the absorption bandwidth can be enlarged by varying the size, position and inter-particle distance will complicate the control of subsequent photocatalysis. **We propose to employ high-order or hybrid plasmonic modes of metallic nanostructures to extend the bandwidth of photon absorption, covering a wide spectral range in the visible and infrared, so that the solar energy conversion efficiency could be drastically enhanced.** One design is schematically shown in Figure 18a. It consists of periodic stripes made of metal multilayers that are separated by semiconductors, or metal-organic frameworks (MOFs). The semiconductor or MOFs function as photocatalytically active materials, while the metal supports plasmonic resonance. Two adjacent metal layers couple with each other, supporting a hybrid plasmonic mode under transverse magnetic (TM) illumination. By cascading metallic layers with different widths, we can increase the absorption bandwidth to over 400 nm in the optical regime (Figure 18b). Lastly, from Figure 2c-e, the local electric field (|E|) is amplified approximately 20-fold. These features are highly useful to harvest photons over an extremely broad solar spectrum and benefit the subsequent photon-chemical conversion process.

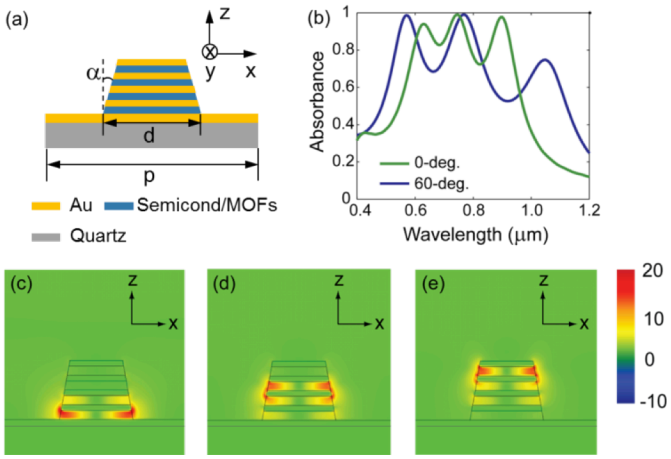

Figure 18. Plasmonic nanostructures for broadband perfect absorption. (a) Cross-sectional view of the 2D periodic plasmonic nanostructure. (b) Absorbance for normal incidence and oblique incidence. (c)-(d) Electric field plot for resonant wavelength at 0.62, 0.72 and 0.9 μm, respectively, showing the large local field enhancement over 20 times.

Plasmonics Enhanced Photocatalytic and Electrochemical Reactions

Plasmonics Enhanced Photocatalytic and Electrochemical Reactions Preliminary experiments were specifically designed to test the above hypothesis by choosing reductive charge transfer reactions such as oxygen reduction and hydrogen evolution in both aqueous and non- aqueous medium. The goal was to take a well known reductive process with conventional quasi outer sphere charge transfer steps such as the well known ORR one electron step to super-oxide in non-aqueous electrolyte. As studied extensively in Mukerjee's group,[64] this one electron step depends intimately on the donor acceptor properties of the solvent. As shown below, our experiments involved using glassy carbon substrate (GC) with and without the dispersed plasmonic nano-particles (20 Å, mono-dispersed Au). Use of dimethyl sulfoxide was specifically chosen in order to drive the reaction towards an outer sphere charge transfer. This aspect is well described in our previous report.[64]As evident from Figure 19, the induction of gold nanoparticles with illumination of laser at 532 nm wavelength drastically affects the oxygen

reduction via enhancement of both super-oxide (first reduction peak) and even subsequent reduction to peroxide. Such a delineation clearly demonstrates the potential of plasmonic enhancement for solar-electrochemical energy conversion.

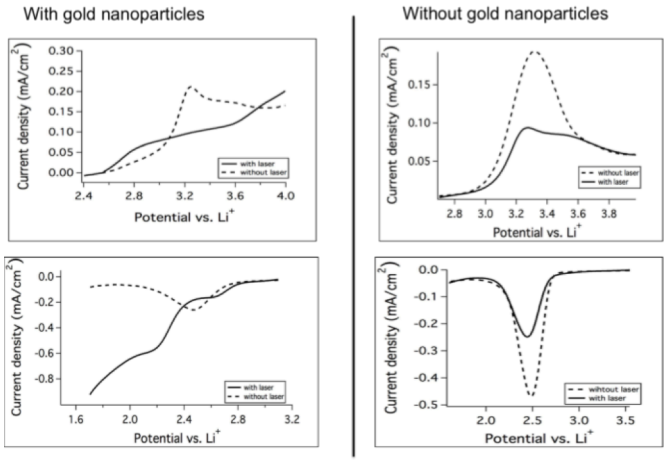

Figure 19. ORR/OER scans on a GC electrode RDE in situ cell enabled for laser exposure. Scan rate 50 mV/s, DMSO/$LiPF_6$ with and without Au (20 Å, see inset) and laser exposure. Note the two emergent reduction peaks with Au on GC exposed to laser radiation.

References

[1] Blomen LJMJ, Mugerwa MN. Fuel Cell Systems. New York: Plenum Press; 1993.
[2] Li YS, Zhao TS, Liang ZX. Performance of alkaline electrolyte-membrane based direct ethanol fuel cells. J Power Sources. 2009;187:387-92.
[3] Fujiwara N, Siroma Z, Yamazaki S-i, Ioroi T, Senoh H, Yasuda K. Direct ethanol fuel cells using an anion exchange membrane. J Power Sources. 2008;185:621-6.
[4] Hou H, Sun G, He R, Wu Z, Sun B. Alkali doped polybenzimidazole membrane for high performance alkaline direct ethanol fuel cell. J Power Sources. 2008;182:95-9.
[5] Coutanceau C, Demarconnay L, Lamy C, Leger J-M. Development of electrocatalysts for solid alkaline fuel cell (SAFC). J Power Sources. 2006;156:14-9.
[6] Kim J, Momma T, Osaka T. Cell performance of Pd-Sn catalyst in passive direct methanol alkaline fuel cell using anion exchange membrane. J Power Sources. 2009;189:999-1102.
[7] Matsuoka K, Iriyama Y, Abe T, Matsuoka M, Ogumi Z. Alkaline direct alcohol fuel cells using an anion exchange membrane. J Power Sources. 2005;15-:27-31.
[8] Yu EH, Scott K. Direct methanol alkaline fuel cells with catalysed anion exchange membrane electrodes. J Appl Electrochem. 2005;35:91-6.
[9] Yu EH, Scott K. Development of direct methanol alkaline fuel cells using anion exchange membranes. J Power Sources. 2004;137:248-56.
[10] Jaouen F, Proietti E, Lefevre M, Chenitz R, Dodelet J-P, Wu G, et al. Recent advances in non-precious metal catalysis for oxygen-reduction reaction in polymer electrolyte fuel cells. Energy Environ Sci. 2011;4:114-30.
[11] Dodelet J-P. Oxygen Reduction in PEM Fuel Cell Conditions: Heat-Treated Non-Precious Metal-N_4 Macrocycles and Beyond. In: Zagal JH, Bedioui F, Dodelet J-P, editors. N4-Macrocyclic Metal Complexes: Springer; 2006. p. 83-139.
[12] Wu G, Johnston CM, Mack NH, Artyushkova K, Ferrandon M, Nelson M, et al. Synthesis-structure-performance correlation for polyaniline-Me-C non-precious metal cathode catalysts for oxygen reduction in fuel cells. Journal of Materials Chemistry. 2011;21:11392-405.
[13] Jaouen F, Herranz J, Lefèvre M, Dodelet J-P, Kramm UI, Herrmann I, et al. Cross-Laboratory Experimental Study of Non-Noble-Metal Electrocatalysts for the Oxygen Reduction Reaction. ACS Applied Materials & Interfaces. 2009;1:1623-39.
[14] Lefevre M, Proietti E, Jaouen F, Dodelet J-P. Iron-Based Catalysts with Improved Oxygen Reduction Activity in Polymer Electrolyte Fuel Cells. Science (Washington, DC, U S). 2009;324:71-4.
[15] Proietti E, Jaouen F, Lefevre M, Larouche N, Tian J, Herranz J, et al. Iron-based cathode catalyst with enhanced power density in polymer electrolyte membrane fuel cells. Nature communications. 2011;2:416.
[16] Wu G, More KL, Johnston CM, Zelenay P. High-performance electrocatalysts for oxygen reduction derived from polyaniline, iron, and cobalt. Science (Washington, DC, U S). 2011;332:443-7.
[17] Zagal JH. Fundamental Aspects on the Catalytic Activity of Metallomacrocyclices for the Electrochemical Redcution of O_2. In: Zagal JH, Bedioui F, Dodelet J-P, editors. N4-Macrocyclic Metal Complexes: Springer; 2006. p. 41-75.
[18] Oyaizu K, Murata H, Yuasa M. Macrocycles for Fuel Cell Cathodes

Molecular Catalysts for Energy Conversion. In: Okada T, Kaneko M, editors.: Springer Berlin Heidelberg; 2009. p. 139-62.
[19] Xu Y, Shao M, Mavrikakis M, Adzic RR. Recent Developments in the Electrocatalysis of the O_2 Reduction Reaction. In: Koper MTM, editor. Fuel Cell Catalysis A Surface Science Approach: John Wiley & Sons, Inc.; 2009.

[20] Reed CA, Cheung SK. On the bonding of FeO2 in hemoglobin and related dioxygen complexes. Proceedings of the National Academy of Sciences. 1977;74:1780-4.
[21] Nakashima H, Hasegawa J-Y, Nakatsuji H. On the reversible O2 binding of the Fe–porphyrin complex. Journal of Computational Chemistry. 2006;27:426-33.
[22] Zagal JH, Gulppi M, Isaacs M, Cardenas-Jiron G, Aguirre MJ. Linear versus volcano correlations between electrocatalytic activity and redox and electronic properties of metallophathalocyanines. Electrochim Acta. 1998;44:1349-57.
[23] Beck F. The redox mechanism of the chelate-catalyzed oxygen cathode. J Appl Electrochem. 1977;7:239-45.
[24] Liao M-S, Scheiner S. Electronic structure and bonding in metal porphyrins, metal = Fe, Co, Ni, Cu, Zn. J Chem Phys. 2002;117:205-19.
[25] Kadish KM, Van Caemelbecke E, Royal G. Electrochemistry of metalloporphyrins in nonaqueous media. In: Kadish KM, Smith KM, Guilard R, editors. Porphyrin Handbook: Academic Press; 2000. p. 1-114.
[26] Yamashige H, Matsuo S, Kurisaki T, Perera RCC, Wakita H. Electronic Structure Analysis of Iron(III)-Porphyrin Complexes by X-ray Absorption Spectra at the C, N and Fe K-Edges. Analytical Sciences. 2005;21:309-14.
[27] Yamazaki S, Yamada Y, Ioroi T, Fujiwara N, Siroma Z, Yasuda K, et al. Estimation of specific interaction between several Co porphyrins and carbon black: its influence on the electrocatalytic O2 reduction by the porphyrins. Journal of Electroanalytical Chemistry. 2005;576:253-9.
[28] Ljubisa R. Surface Chemical and Electrochemical Properties of Carbons. Carbons for Electrochemical Energy Storage and Conversion Systems: CRC Press; 2009. p. 163-219.
[29] Burg P, Cagniant D. Characterization of Carbon Surface Chemistry. Chemistry & Physics of Carbon: CRC Press; 2007. p. 129-75.
[30] Darmstadt H, Roy C. Surface spectroscopic study of basic sites on carbon blacks. Carbon. 2003;41:2662-5.
[31] Bard AJ. Inner-Sphere Heterogeneous Electrode Reactions. Electrocatalysis and Photocatalysis: The Challenge. J Am Chem Soc. 2010;132:7559-67.
[32] Ramaswamy N, Mukerjee S. Influence of Inner- and Outer-Sphere Electron Transfer Mechanisms during Electrocatalysis of Oxygen Reduction in Alkaline Media. The Journal of Physical Chemistry C. 2011;115:18015-26.
[33] Ramaswamy N, Allen RJ, Mukerjee S. Electrochemical Kinetics and X-ray Absorption Spectroscopic Investigations of Oxygen Reduction on Chalcogen-Modified Ruthenium Catalysts in Alkaline Media. The Journal of Physical Chemistry C. 2011;115:12650-64.
[34] Bocarsly AB, Barton EE. Chemical carbon mitigation: Using light to convert carbon dioxide to methanol and higher order alcohols. Abstracts of Papers, 237th ACS National Meeting, Salt Lake City, UT, United States, March 22-26, 2009. 2009:INOR-632.
[35] Kim I, Han Oc H, Chae Seen A, Paik Y, Kwon S-H, Lee K-S, et al. Catalytic reactions in direct ethanol fuel cells. Angewandte Chemie (International ed in English). 2011;50:2270-4.
[36] Antolini E. Catalysts for direct ethanol fuel cells. J Power Sources. 2007;170 1–12.
[37] Corma A, Diaz-Cabanas MJ, Martinez-Triguero J, Rey F, Rius J. A large-cavity zeolite with wide pore windows and potential as an oil refining catalyst. Nature (London, United Kingdom). 2002;418:514-7.
[38] Lai SCS, Koper MTM. Electro-oxidation of ethanol and acetaldehyde on platinum single-crystal electrodes. Faraday Discuss. 2008;140:399-416.
[39] Wang H, Jusys Z, Behm RJ. Ethanol electro-oxidation on carbon-supported Pt, PtRu and Pt3Sn catalysts: A quantitative DEMS study. Journal of Power Sources. 2006;154:351-9.
[40] Jiang L, Colmenares L, Jusys Z, Sun GQ, Behm RJ. Ethanol electrooxidation on novel carbon supported Pt/SnOx/C catalysts with varied Pt:Sn ratio. Electrochimica Acta. 2007;53:377-89.

[41] Wang H, Zhao Y, Jusys Z, Behm RJ. Ethylene glycol electrooxidation on carbon supported Pt, PtRu and Pt3Sn catalysts-A comparative DEMS study. Journal of Power Sources. 2006;155:33-46.
[42] Lai Stanley CS, Koper Marc TM. Ethanol electro-oxidation on platinum in alkaline media. Phys Chem Chem Phys. 2009;11:10446-56.
[43] Tripkovic AV, Popovic KD, Grgur BN, Blizanac B, Ross PN, Markovic NM. Methanol electrooxidation on supported Pt and PtRu catalysts in acid and alkaline solutions. Electrochim Acta. 2002;47:3707-14.
[44] Rao V, Hariyanto, Cremers C, Stimming U. Investigation of the ethanol electro-oxidation in alkaline membrane electrode assembly by differential electrochemical mass spectrometry. Fuel Cells (Weinheim, Germany). 2007;7:417-23.
[45] Mondelli C, Grunwaldt J-D, Ferri D, Baiker A. Role of Bi promotion and solvent in platinum-catalyzed alcohol oxidation probed by in situ X-ray absorption and ATR-IR spectroscopy. Physical Chemistry Chemical Physics. 2010;12:5307-16.
[46] Mondelli C, Ferri D, Grunwaldt J-D, Krumeich F, Mangold S, Psaro R, et al. Combined liquid-phase ATR-IR and XAS study of the Bi-promotion in the aerobic oxidation of benzyl alcohol over Pd/Al2O3. J Catal. 2007;252:77-87.
[47] Grunwaldt J-D, Caravati M, Baiker A. Oxidic or Metallic Palladium: Which Is the Active Phase in Pd-Catalyzed Aerobic Alcohol Oxidation? J Phys Chem B. 2006;110:25586-9.
[48] Haan JL, Masel RI. Recent progress in improving the oxidation of formic acid on high surface area platinum and palladium catalysts: surface alloying and pH effects. ECS Trans. 2008;16:627-38.
[49] Cuesta A. Atomic Ensemble Effects in Electrocatalysis: The Site-Knockout Strategy. ChemPhysChem. 2011;12:2375-85.
[50] Xu C, Shen PK, Ji X, Zeng R, Liu Y. Enhanced activity for ethanol electrooxidation on Pt-MgO/C catalysts. Electrochemistry Communications. 2005;7:1305-8.
[51] Xu C, Shen Pei K. Novel Pt/CeO2/C catalysts for electrooxidation of alcohols in alkaline media. Chemical communications (Cambridge, England). 2004:2238-9.
[52] Bai Y, Wu J, Xi J, Wang J, Zhu W, Chen L, et al. Electrochemical oxidation of ethanol on Pt-ZrO2/C catalyst. Electrochemistry Communications. 2005;7:1087-90.
[53] Kowal A, Li M, Shao M, Sasaki K, Vukmirovic MB, Zhang J, et al. Ternary Pt/Rh/SnO2 electrocatalysts for oxidizing ethanol to CO2. Nat Mater. 2009;8:325-30.
[54] Schmiemann U, Mueller U, Baltruschat H. The influence of the surface structure on the adsorption of ethene, ethanol and cyclohexene as studied by DEMS. Electrochimica Acta. 1995;40:99-107.
[55] Gomes Janaina F, Busson B, Tadjeddine A. SFG study of the ethanol in an acidic medium--Pt(110) interface: effects of the alcohol concentration. The journal of physical chemistry B. 2006;110:5508-14.
[56] Martin P, Monzyk B, Burckle E, Busch J, Gilbert R, Dasse K. Progress towards development of a photolytic artificial lung. Materials Science and Engineering: B. 2005;119:246-51.
[57] Vollmer AP, Probstein RF, Gilbert R, Thorsen T. Development of an integrated microfluidic platform for dynamic oxygen sensing and delivery in a flowing medium. Lab on a Chip. 2005;5:1059-66.
[58] Gilbert RJ, Carleton LM, Dasse KA, Martin PM, Williford RE, Monzyk BF. Photocatalytic generation of dissolved oxygen and oxyhemoglobin in whole blood based on the indirect interaction of ultraviolet light with a semiconducting titanium dioxide thin film. Journal of Applied Physics. 2007;102:073512.
[59] Shen M, Henderson MA. Identification of the active species in photochemical hole scavenging reactions of methanol on TiO2. The Journal of Physical Chemistry Letters. 2011;2:2707-10.
[60] Mukherjee S, Libisch F, Large N, Neumann O, Brown LV, Cheng J, et al. Hot electrons do the impossible: plasmon-induced dissociation of H2 on Au. Nano letters. 2012;13:240-7.
[61] Mubeen S, Lee J, Singh N, Krämer S, Stucky GD, Moskovits M. An autonomous photosynthetic device in which all charge carriers derive from surface plasmons. Nature nanotechnology. 2013;8:247-51.

[62] Zentgraf T, Liu Y, Mikkelsen MH, Valentine J, Zhang X. Plasmonic luneburg and eaton lenses. Nature nanotechnology. 2011;6:151-5.
[63] Liu Y, Palomba S, Park Y, Zentgraf T, Yin X, Zhang X. Compact magnetic antennas for directional excitation of surface plasmons. Nano letters. 2012;12:4853-8.
[64] Trahan MJ, Jia Q, Mukerjee S, Plichta EJ, Hendrickson MA, Abraham K. Cobalt phthalocyanine catalyzed lithium-air batteries. Journal of The Electrochemical Society. 2013;160:A1577-A86.